bioRxiv preprint doi: https://doi.org/10.1101/2021.11.12.468419; this version posted November 13, 2021. The copyright holder for this preprint (which was not certified by peer review) is the author/funder. All rights reserved. No reuse allowed without permission.

hNOP2/NSUN1 Regulates Ribosome Biogenesis through Stabilization of snoRNP Complexes and Cytosine-5 Methylation of 28S rRNA.

Han Liao[1], Anushri Gaur[1], Hunter McConie[1], Amirtha Shekar[1], Karen Wang[2], Jeffrey T. Chang[1], Ghislain Breton[1], and Catherine Denicourt[1, 3, *]

[1] Department of Integrative Biology and Pharmacology, McGovern Medical School, The University of Texas Health Science Center, Houston, TX 77030, USA
[2] Wiess College, Rice University, Houston, TX 77251, USA
[3] Lead Contact

*Correspondence should be addressed to:

Catherine Denicourt
The University of Texas HSC-Houston
6431 Fannin St. MSE R368
Houston, TX 77030
Phone: 713-500-5696
FAX: 713-500-7444
Email: Catherine.Denicourt@uth.tmc.edu

Keywords: NOP2/NSUN1, RNA methyltransferases, 5-Methylcytosine, miCLIP-seq, rRNA processing, ribosome biogenesis, box C/D snoRNAs, vault RNA 1.2 (vtRNA1.2).

bioRxiv preprint doi: https://doi.org/10.1101/2021.11.12.468419; this version posted November 13, 2021. The copyright holder for this preprint (which was not certified by peer review) is the author/funder. All rights reserved. No reuse allowed without permission.

ABSTRACT

5-Methylcytosine (m^5C) is a base modification broadly found on a variety of RNAs in the human transcriptome. In eukaryotes m^5C is catalyzed by enzymes of the NSUN family, which is composed of seven members in humans (NSUN1-7). NOP2/NSUN1 has been mostly characterized in budding yeast as an essential ribosome biogenesis factor required for the deposition of m^5C on the 25S rRNA. Although human NOP2/NSUN1 has been known to be an oncogene overexpressed in several types of cancer, its functions remain poorly characterized. To define the roles of human NOP2/NSUN1, we used an miCLIP-seq approach to identify its RNA substrates. Our analysis reveals that vault RNA 1.2 and rRNA are NOP2/NSUN1-specific methylated targets and we further confirm by bisulfite sequencing that NOP2/NSUN1 is responsible for the deposition of m^5C at residue 4447 on the 28S rRNA. Depletion of NOP2/NSUN1 impairs cell proliferation, rRNA processing and 60S ribosome biogenesis. Additionally, we find that NOP2/NSUN1 binds to the 5'ETS region of the pre-rRNA transcript and regulates pre-rRNA processing in part through non-catalytic complex formation with box C/D snoRNAs. Our study identifies for the first time the RNA substrates of human NOP2/NSUN1 and reveals additional functions in rRNA processing beyond catalyzing m^5C base modification.

bioRxiv preprint doi: https://doi.org/10.1101/2021.11.12.468419; this version posted November 13, 2021. The copyright holder for this preprint (which was not certified by peer review) is the author/funder. All rights reserved. No reuse allowed without permission.

INTRODUCTION

Post-transcriptional chemical modification of RNA has emerged in recent years to be an important regulatory mode of gene expression. Over 150 distinct types of modifications have been found to decorate cellular RNAs, of which ribosomal RNA (rRNA) and transfer RNA (tRNA) are the most heavily modified (1). All four RNA bases and the ribose sugar can be targeted for modification, expanding the chemical properties of RNA nucleotides and hence, directly influencing RNA structure (2), stability (3), splicing (4), cellular localization (5) and interactions with RNA-binding proteins (2,6). The recent findings of the dynamicity and reversibility of RNA modifications has highlighted their involvement in crucial biological processes, including development (7), cell fate determination (8), pathogen infection (9-11) and stress response (12,13).

C5 methylation of cytosines (5-methylcytosine or m^5C) is a common modification found in a wide variety of RNA molecules that ranges from ribosomal RNAs (rRNAs), transfer RNAs (tRNAs), messenger RNAs (mRNAs), vault RNAs (vtRNAs) to divers non-coding RNAs (5,14-17). In eukaryotes, m^5C modification on RNA is catalyzed by the members of the NOL1/NOP2/SUN domain family of S-adenosylmethionine (SAM)-dependent methyltransferases (NSUN1 to 7), as well as the DNA methyltransferase homologue DNMT2. NOP2/NSUN1, NSUN2, and NSUN5 are conserved in all eukaryotes, while the other members of the family (NSUN3/4/6/7) are only found in higher eukaryotes (3). The biological impact and extent of RNA cytosine methylation are not completely understood. However, the functional characterizations NSUN proteins as well as the identification of their RNA substrates have started to uncover several important roles played in the regulation of nuclear and mitochondrial gene expression (14,18,19). Mutations and changes in expression levels of genes coding for several NSUN proteins have been linked with diverse human diseases ranging from neurological disorders (20) to cancer (21-23), highlighting the importance of further characterizing this family of RNA methyltransferases.

NOP2/NSUN1 was originally identified in humans as p120, a proliferating-cell nucleolar antigen found overexpressed in a variety of rapidly dividing cells and malignant cancers (21,22,24-34). NOP2/NSUN1 also appears to harbor oncogenic function as its overexpression is sufficient to increase proliferation and confer tumorigenic potential *in vivo* (35). Studies in budding yeast have shown that NOP2/NSUN1 is an essential protein required for pre-rRNA processing and 60S ribosome subunit synthesis. In *S. cerevisiae*, the 25S rRNA (28S in human) of the large subunit contains two m^5Cs at positions 2278 and 2870, which respectively lie at the inter-subunit bridge and in close proximity to the peptidyl-transferase center of the ribosome (36). m^5C has been proposed to stabilize rRNA folding for the formation these functional domains, as it promotes base stacking and increases the stability of hydrogen bonds with guanine (37). NSUN5/Rcm1 methylates C2278 and the human equivalent at C3782 (23,36), whereas NOP2/NSUN1 has only been shown to methylate C2870 in yeast. A cytosine at position 4447 in human 28S rRNA is known to be methylated (38,39) and NOP2/NSUN1 is predicted to catalyze this modification based on homology and functional complementation experiments in

bioRxiv preprint doi: https://doi.org/10.1101/2021.11.12.468419; this version posted November 13, 2021. The copyright holder for this preprint (which was not certified by peer review) is the author/funder. All rights reserved. No reuse allowed without permission.

yeast (40). Recent studies in *C. elegans* have suggested, but not directly demonstrated, that NOP2/NSUN1 methylates the 26S rRNA at position C2982, which is predicted to be the equivalent of human C4447 (41). Although NOP2/NSUN1-dependent deposition of m^5C into rRNAs has been assessed in budding yeast and worms, little is known about the roles and spectrum of substrates of NOP2/NSUN1 in human cells.

Here, we utilized methylation individual-nucleotide-resolution crosslinking and immunoprecipitation-sequencing (miCLIP-seq) to identify methylation targets of NOP2/NSUN1 in human cells. We identify vault RNA 1.2 (vtRNA1.2) and rRNA as NOP2/NSUN1-specific methylated targets and confirmed the deposition of m^5C at residue 4447 of the 28S rRNA by RNA bisulfite sequencing. Interestingly, we also find that in addition to site specific methylation of the 28S rRNA, NOP2/NSUN1 also regulates pre-rRNA processing through non-catalytic complex formation with box C/D snoRNAs. Our study identifies for the first time the spectrum of RNA bound by NOP2/NSUN1 and highlights additional functions in ribosome biogenesis beyond catalyzing rRNA substrate methylation.

MATERIALS AND METHODS

Reagents

Reagents and kits used in this study were: Amersham Hybond N+ nylon membrane (RPN303B, GE healthcare), BCA kit (23225, Pierce), Biotinylated cytidine (bis)phosphate (NU-1706-Bio, Jena Bioscience), Immun-Star AP substrate (1705018, Bio-Rad), iTaq universal SYBR green SuperMix (1725125, Bio-Rad), Lipofectamine RNAi Max (13778075, Invitrogen), Monarch RNA cleanup kit (T2030L, NEB), Murine RNase inhibitor (M0314L, NEB), Nitrocellulose membrane (10600008, GE Healthcare), Protease inhibitors cocktail (78437, Thermo Scientific), Protein G Dynabeads (10003D, Invitrogen), Protein G agarose beads (101242, Invitrogen), Q5 2X master mix (M0492S, NEB), Q5 Site-Directed Mutagenesis Kit (E0554, NEB), RevertAid reverse transcriptase (EP0441, Thermo Scientific), Streptavidin-alkaline phosphatase conjugate (434322, Invitrogen), Streptavidin-IR800 (926-32230, LI-COR), SuperScript III (18080044, Invitrogen), Taq polymerase (M0273S, NEB), Random hexamer primers (SO142, Thermo Scientific), Thiazolyl blue tetrazolium bromide (MTT, T3450, Biosynth), TriZol reagent (15596018, Invitrogen), TurboDNase (AM2239, Invitrogen), Puromycin (P8833, Sigma). Antibodies used were: NOP2 (A302-018A, Bethyl), FLAG (F1804, Sigma), FBL (A303-891A, Bethyl), NOP56 (PA5-78329, Invitrogen), p53 (SC-126, Santa Cruz Biotechnology), p21 (556430, BD Biosciences), GAPDH (47724, Santa Cruz Biotechnology), Puromycin (PMY-2A4-s, DSHB), Normal rabbit IgG (NI01, Millipore).

Biological resources

HCT116 wildtype (WT), HCT116 p53-/-, and HEK293T were purchased from ATCC. Lentiviral plasmid empty backbone pLKO-Tet-On was obtained from Addgene (21915). Plasmid p3XFLAG -CMV-7.1 was obtained from Sigma (E7533).

bioRxiv preprint doi: https://doi.org/10.1101/2021.11.12.468419; this version posted November 13, 2021. The copyright holder for this preprint (which was not certified by peer review) is the author/funder. All rights reserved. No reuse allowed without permission.

Data Availability/Sequence Data Resources

The datasets generated and/or analyzed during the current study are publicly available at the GEO genomics data repository (accession # pending).

Cell culture and proliferation assay

HCT116 wildtype (WT), HCT116 p53-/-, and HEK293T cells were maintained in high glucose Dulbecco's modified Eagle's medium (DMEM) with 5% fetal bovine serum (FBS), 100 U/ml penicillin, and 100 µg/ml streptomycin under 5% CO_2 atmosphere at 37 ^{o}C. Cells were replated in to 48-well plates at 10 000 cells per well 48 h after siRNA transfection. From 72 h to 168 h after siRNA transfection, cell counts per well were determined using an MTT assay. MTT reagent was added to culture at 0.5 mg/ml and incubated for 4 h. Media was carefully removed and MTT formazan crystals were dissolved by DMSO. MTT formazan concentration, which correlates with cell number, was read at 570 nm.

RNA interference

Synthetic short interfering RNA (siRNA) oligonucleotides (Sigma) were delivered into cells using Lipofectamine RNAi Max with the reverse transfection protocol according to the manufacturer's instructions. Briefly, 20 nM of siRNA oligonucleotide was incubated with 6 µl of Lipofectamine RNAi Max in a 6-well plate format. Cell suspension (150 000 cells/well) was then added to the well containing the transfection mixture. The following siRNA sequences were used: Control (non-targeting scramble): 5'-GAUCAUACGUGCGAUCAGATT-3', siNOP2#1: 5'-CACCUGUUCUAUCACAGUATT-3', siNOP2#2: 5'-GCAACGAUCACCUAAAUUATT-3'.

Lentivirus construction and virus production

NOP2 shRNA sequences (oligo sequence available in Supplementary Table 1) were cloned into pLKO-Tet-On as described by Wiederschain *et al* (42). Lentivirus was produced by co-transfecting HEK-293T cells with pLKO-Tet-On-shNop2, pMDL, pVSVG, pREV in a ratio of 3:1:1:1 (43). Media was renewed 24h after transfection and virus containing media was collected 48h and 72h after transfection.

Exogenous expression of wildtype and C459A mutant NOP2

Wildtype NOP2/NSUN1 gene was cloned into p3XFLAG -CMV-7.1 plasmid. The C459A mutation was created using the NEB Q5 Site-Directed Mutagenesis Kit and primers listed in Supplementary Table 1. Sequences of NOP2/NSUN1 WT and C459A constructs were confirmed by Sanger sequencing (Genewiz).

RNA extraction and Northern blot analysis

bioRxiv preprint doi: https://doi.org/10.1101/2021.11.12.468419; this version posted November 13, 2021. The copyright holder for this preprint (which was not certified by peer review) is the author/funder. All rights reserved. No reuse allowed without permission.

Total RNA was extracted using TriZol reagent following manufacturer's instruction. 2.5 µg of total RNA was separated on 0.8% formaldehyde denaturing agarose gel or 10% 8M urea-PAGE gel and transferred to Amersham Hybond N+ nylon membrane. RNA was crosslinked to membrane by 120 mJ/cm^2 UV exposure. Membrane was pre-hybridized in hybridization buffer (0.6 M NaCl, 60 mM sodium citrate pH 7, 0.5% SDS, 0.1% BSA, 0.1% polyvinyl pyrrolidone, 0.1% ficoll 400) at 50 ^{o}C for 1h and hybridized with 20nM biotin-labeled probe in fresh hybridization buffer overnight. Probe was detected using streptavidin-alkaline phosphatase conjugate and Immun-Star AP substrate. Probes for Northern blot are listed in Supplementary Table 1. ImageJ was used for densitometry quantification analysis of each blot.

RNA immunoprecipitation (RNA-IP) and RT-qPCR

To assess NOP2/NSUN1 or Nop56 association to snoRNAs by RNA-IP, cells were lysed in lysis buffer (1% NP-40, 50 mM Tris-HCl pH 8, 150 mM NaCl, 5 mM EDTA, 100 U/ml murine RNase inhibitor, 1X protease inhibitors cocktail) on ice for 15 min and triturated 10 times through a 27-gauge needle. The lysates were cleared by centrifugation at 15000 g for 10 min at 4 ^{o}C and the supernatant was incubated with 10 µl of protein G Dynabeads pre-bound with 1 µg of antibody or normal IgG. After 2 h incubation, beads were washed 5 times with cold high salt wash buffer (1% NP-40, 50 mM Tris-HCl pH 8, 500 mM NaCl, 5 mM EDTA) and 2 times with no salt wash buffer (20 mM Tris-HCl pH 7.4, 0.2% Tween-20). Beads were treated with DNase and followed by proteinase K. Immuno-precipitated RNA was extracted using TriZol reagent. RNA samples were reverse transcribed using RevertAid reverse transcriptase and random hexamer. qPCR was performed with 500 nM specific primer mix and iTaq universal SYBR green SuperMix on a C1000 Touch CFX-384 real-time qPCR system (Bio-Rad). Primer efficiency test was performed by using serial dilution of cDNA made from 1 µg total RNA. Efficiency was calculated using the following formula: efficiency = 10 ^ (-1/Slope of standard curve). Primers for qPCR are listed in Supplementary Table 1.

Immunoprecipitation and Immunoblotting

For co-immunoprecipitation analysis, cells were lysed in ELB buffer (0.5% NP-40, 50 mM HEPES pH 7.2, 250 mM NaCl, 2 mM EDTA, 1X protease inhibitors cocktail) on ice for 15 min. The lysates were cleared by centrifugation at 15000 g for 10 min at 4 ^{o}C and the supernatant was incubated with 20 µl of protein G agarose beads pre-bound with 1 µg of antibody or normal IgG. After 2 h incubation, beads were washed 4 times with ELB buffer and re-suspended in 15 µl 2X protein loading dye (4% SDS, 0.25 M Tris-HCl pH 6.8, 20% glycerol, 3% beta-mercaptoethanol, 0.04% bromophenol blue). For total protein extraction, cells were washed with PBS, harvested by scraping, and lysed in RIPA buffer (25mM Tris-HCl pH 7.6, 150mM NaCl, 1% NP-40, 1% Triton X-100, 1% sodium deoxycholate, and 0.1% SDS) plus protease inhibitors cocktail for 15 minutes on ice. Lysates were cleared by centrifugation at 22000 x g for 10 minutes at 4°C. Protein concentrations were evaluated with the BCA kit. Proteins were separated on SDS-poly-acrylamide gel electrophoresis (SDS-PAGE) and transferred to a nitrocellulose membrane.

bioRxiv preprint doi: https://doi.org/10.1101/2021.11.12.468419; this version posted November 13, 2021. The copyright holder for this preprint (which was not certified by peer review) is the author/funder. All rights reserved. No reuse allowed without permission.

Polysome preparation

HCT116 cells were infected with doxycycline-inducible NOP2/NSUN1 shRNA-expressing lentivirus. After puromycin selection, cells were treated with 200 ng/ ml doxycycline for 4 days before harvest to induced shRNA expression. Non-treated cells were used as control. Polysome profile was done as described previously by Simsek *et al.,* (44). In brief, cells were treated with 100 μg/ml cycloheximide for 5 min and lysed in polysome buffer (25 mM Tris-HCl pH 7.5, 150 mM NaCl, 15 mM MgCl2, 8% glycerol, 1% Triton X-100, 0.5% sodium deoxycholate, 1 mM DTT, 100 ug/ml cycloheximide, 100 U/ml murine RNase inhibitor (NEB), 25 U/ml TurboDNase, 1X protease inhibitor cocktail). Lysate was cleared by a serial of centrifugation, loaded on 10%-50% sucrose gradient, and ultra-centrifuged at 40 000 RPM for 2.5h at 4ºC with a Beckman Ti-41 swing rotor. Fractions were collected using a piston gradient fractionator (BioComp).

Sucrose gradient density centrifugation for co-sedimentation assay

HCT116 cells were suspended in fractionation buffer (150 mM NaCl, 20 mM HEPES-KOH pH 7.9, 0.5 mM DTT, 100 U/ml murine Rnase inhibitor, 1X protease inhibitor cocktail) and lysed by sonication. TritonX-100 was added to the lysate to a final concentration of 0.2% and the lysates were cleared by centrifugation. The supernatant was loaded on 10%-30% sucrose gradient, and ultra-centrifuged at 36000 RPM for 3h at 4ºC with a Beckman Ti-41 swing rotor. Fractions were collected using a piston gradient fractionator (BioComp). Protein from each fraction was extracted as described by Pestov *et al.,* (45) for Western blot analysis.

Puromycin labeling assay

Seventy-two hours after siRNA transfection, HCT116 WT cells were replated into 6-well plate at 8 x 10^5 cells/well and incubated for another 12 h. Cells were treated with 5 μg/ml puromycin for 0, 15, and 30 min and immediately harvested for Western blot analysis using an anti-puromycin antibody.

Biotin-labelling of immunoprecipitated RNA

pCp-Biotin labeling of immunoprecipitated RNA was performed according to (46). Briefly, four million HEK293T cells expressing empty vector, FLAG-NOP2-WT or FLAG-NOP2-C459A were lysed in CLIP buffer (50 mM Tris-HCl pH 7.4, 100 mM NaCl, 1% NP-40, 0.1% SDS, 0.5% sodium deoxycholate, 1X Protease Inhibitor Cocktail) without UV crosslink on ice for 15 min. followed by sonication and digestion with RNase T1 and Turbo DNAse at 37ºC for 5 min. Digested lysates were cleared by centrifugation and immunoprecipitated using 25 μl of protein G Dynabeads pre-bound with 2 μg of anti-FLAG antibody at 4ºC overnight. Samples were washed twice in high salt wash buffer (50 mM Tris-HCl pH 7.4, 1 M NaCl, 1% NP-40, 0.1% SDS, 0.5% sodium deoxycholate, 1 mM EDTA), thrice in wash buffer (20 mM Tris-HCl pH 7.4, 0.2% Tween-20) and RNA was dephosphorylated on beads by Fast-AP and T4 PNK and ligated with biotinylated cytidine (bis)phosphate

bioRxiv preprint doi: https://doi.org/10.1101/2021.11.12.468419; this version posted November 13, 2021. The copyright holder for this preprint (which was not certified by peer review) is the author/funder. All rights reserved. No reuse allowed without permission.

(pCp-Biotin) using T4 RNA ligase. Samples were loaded on 8% SDS-PAGE gel for separation and transferred to a nitrocellulose membrane. Streptavidin-IR800 was used for detecting biotin-labeled RNA and the membrane was scanned using LI-COR Odyssey DLx Imager.

miCLIP-sequencing

The eCLIP-sequencing protocol described by Van Nostrand *et al* (47) was applied with minor modifications. Twenty million cells were lysed in CLIP buffer (50 mM Tris-HCl pH 7.4, 100 mM NaCl, 1% NP-40, 0.1% SDS, 0.5% sodium deoxycholate, 1X Protease Inhibitor Cocktail) without UV crosslink on ice for 15 min. followed by sonication and digestion with RNase T1 and Turbo DNAse at 37ºC for 5 min. Digested lysates were cleared by centrifugation and immunoprecipitated using 100 μl of protein G Dynabeads pre-bound with 10 μg of anti-FLAG antibody at 4ºC overnight. Samples were washed twice in high salt wash buffer (50 mM Tris-HCl pH 7.4, 1 M NaCl, 1% NP-40, 0.1% SDS, 0.5% sodium deoxycholate, 1 mM EDTA), once in wash buffer (20 mM Tris-HCl pH 7.4, 0.2% Tween-20) and RNA was dephosporylated, treated with T4 PNK and ligated to 3' RNA adapter (/5Phos/rArGrArUrCrGrGrArArGrArGrCrArCrArCrGrUrC/3SpC3/) on beads. Samples (including SMinputs) were loaded on 8% SDS-PAGE gel for separation, transferred to a nitrocellulose membrane and RNA was isolated from membrane by cutting a region 75 kDa above NOP2/NSUN1. CLIP and SMinput libraries were prepared as paired-end high-throughput libraries as described in (47) and sent for sequencing on Illumina Hi-Seq 4000 platform (Novogene). Raw sequencing data were adaptor trimmed using CutAdapt (48). Unique molecular identifier (UMI) was appended to the read name using fastp (49). Reads less than 18 nt were discarded. Trimmed reads were aligned to human genome (hg38) and human repetitive elements using family-aware repetitive elements mapping pipeline described by Van Nostrand *et al (46)*. miCLIP peak calling was performed on mapped reads from the above repetitive elements mapping pipeline using Peakachu (https://github.com/tbischler/PEAKachu) with parameter --paired_end --max_insert_size 220. To determine crosslink sites on rRNA, trimmed reads were aligned to 47S rRNA (NR_046235) using Bowtie2 (50) with parameter --no-mixed -a, and deduplicated using UMI-tools (51) with parameter --read-length. Mapping statistics, sequencing depth and read start was obtained using Samtools package (52) and reverse transcription (RT) stops were assigned at the start (+1) sites of Read1 sequence.

Bisulfite-sequencing

Two micrograms of nuclear RNA were incubated with 2.3 M $Na_2S_2O_5$ and 0.57 mM hydroquinone at 70ºC for 5 min followed by 54ºC for 75 min. Converted RNA was extracted using NEB Monarch RNA extraction kit and desulfonated with 1M Tris-HCl pH9 at 37ºC for 1h. RNA was then precipitated in ice cold ethanol. cDNA was made with superscript III reverse transcriptase and random 9-mer. PCR of 28S fragment from position 4178 to 4534 was done using NEB Taq polymerase and target specific primers with Illumina adaptor overhangs. PCR product was purified by gel extraction and sequenced on Mi-Seq platform with 2x250 paired-end mode (Genewiz EZ Amplicon

bioRxiv preprint doi: https://doi.org/10.1101/2021.11.12.468419; this version posted November 13, 2021. The copyright holder for this preprint (which was not certified by peer review) is the author/funder. All rights reserved. No reuse allowed without permission.

sequencing, 130 000 reads/sample were aligned to 28S rRNA in average). The primers used for bisulfite sequencing are listed in Supplementary Table 1. Sequencing reads were aligned to converted reference sequence using Bowtie2 with default settings. Mapping information was retrieved using Samtools package as described previously by Heng (52).

Statistics

Data were shown as mean ± standard deviation. Each dot on dot-bar plot represents an independent biological replicate. Difference between two groups was determined by two-tailed Student's *t* test.

RESULTS

NOP2/NSUN1 binds to rRNA, vtRNA1.2 and snoRNAs

We utilized a miCLIP-sequencing approach to identify NOP2/NSUN1 RNA substrates and map C5-methylated cytosines at nucleotide resolution (16)**.** A characteristic of NSUN methyltransferases is the presence of two catalytic cysteines in their active site. Preceding methylation, a covalent intermediate is first formed between motif VI cysteine and the RNA cytosine pyrimidine ring. After catalysis, release of the methylated RNA depends on the second conserved cysteine located in motif IV (Figure 1A) and mutation of this cysteine has been shown to result in a stable covalent protein-RNA intermediate (3,53,54). miCLIP takes advantage of this particularity and allows NSUN proteins with a mutated cysteine (motif IV) to be immunoprecipitated with a covalently trapped RNA substrate without UV crosslinking (Figure 1B) (16). Mutation of NOP2/NSUN1 conserved motif IV cysteine (C459A) resulted in the stabilization of covalently linked RNA intermediates as evidenced by a shift in molecular weight of immunoprecipitated FLAG-tagged C459A mutant compared with WT (Figure 1C). Labeling of immunoprecipitated FLAG-NOP2/NSUN1 WT and C459A with pCp-Biotin followed by detection with fluorescence imaging of streptavidin conjugated-IR800 confirmed the presence of trapped protein-RNA complexes (Figure 1D, high exposure panel). Although not to the same extent as for the mutant, immunoprecipitated FLAG-WT also showed RNA labeling above control level, suggesting that NOP2/NSUN1 may be tightly bound to a subpopulation of RNAs.

Following limited RNase digestion and immunoprecipitation with a FLAG antibody, co-precipitated RNA from Mock, WT and C459A mutant complexes (as well as their respective paired size-matched input (SMInput)) were purified by separation on SDS-PAGE, membrane transferred, and protein-RNA complexes from a 75 kDa region above NOP2/NSUN1 were excised (Figure 1E). Recovered RNA was further prepared into paired-end high-throughput libraries for sequencing on Illumina Hi-Seq 4000 platform. Only samples from biological duplicates of WT, C459A mutant and respective paired SMInput were processed for sequencing as the Mock immunoprecipitated samples did not recover enough RNA to be amplified for library preparation. Reads were processed using a modified eCLIP-seq pipeline (46). The numbers of reads identified as binding site in miCLIP were normalized to SMInput and SMInput-normalized significance and fold enrichment were calculated (Supplementary Table 2).

bioRxiv preprint doi: https://doi.org/10.1101/2021.11.12.468419; this version posted November 13, 2021. The copyright holder for this preprint (which was not certified by peer review) is the author/funder. All rights reserved. No reuse allowed without permission.

The majority of miCLIP reads for the C459A mutant (>97%) corresponded to rRNA (Figure 2A), which also showed peaks of significant enrichments when normalized to SMInput (Figure 2B). The remaining reads mostly mapped to different types of non-coding RNAs (ncRNA) where significantly enriched peaks corresponded to vtRNA1.2 and several snoRNAs (1.1%), with U3 (SNORD3) and U8 (SNORD118) being the most represented (Figure 2B). NOP2/NSUN1 C459A mutant bound primarily to C/D box snoRNAs (SNORD), which include U3 and U8. Only a few H/ACA box snoRNAs were found, indicating specificity of interaction for NOP2/NSUN1 with C/D box snoRNAs (Figure 2C, Supplementary Table 2). Surprisingly, most of the reads from WT NOP2/NSUN1 also mapped to rRNA (>98%), followed by C/D box snoRNAs and various ncRNAs (Figure 2A-C, Supplementary Table 2). WT NOP2/NSUN1 did not show any significant enrichment for vtRNA1.2, suggesting it could be a catalytic substrate as it only was found bound by the C459A mutant. Previous studies have shown that RNA that is not crosslinked to protein can transfer to nitrocellulose membranes but this did not add any significant background to the eCLIP profiles (46,55). To confirm the interaction with C/D box snoRNAs, we independently immunoprecipitated FLAG-NOP2/NSUN1 WT and C459A mutant in un-crosslinked CLIP conditions without membrane transfer followed by qRT-PCR analysis. Both WT and mutant showed significant binding enrichment to snoRNAs over Mock sample also immunoprecipitated with FLAG antibody (Supplementary Figure S1). Together, these findings confirm that NOP2/NSUN1 likely forms strong interactions with certain RNAs, which resist the stringent wash conditions utilized during the CLIP purification steps.

NOP2/NSUN1 methylates 28S rRNA at C4447

Human rRNA is transcribed by RNA Pol I as a long precursor transcript (47S) that undergoes a complex series of cleavage and modification steps to generate the mature 18S, 28S, and 5.8S rRNAs (56,57). 5S rRNA is separately transcribed by RNA Pol III (58). Alignment of the CLIP reads to the 47S precursor rRNA revealed that both NOP2/NSUN1 WT and C459A mutant have a similar and specific binding pattern to the 5' external transcribed spacer (5'ETS) region containing the 01/A', A0 and 1 endonucleolytic processing cleavage sites (Figure 3A). Interestingly, only the C459A mutant showed a distinct enrichment peak on the 28S rRNA that mapped exactly at C4447, which corresponds to the predicted NOP2/NSUN1 methylation site based on homology to the yeast counterpart (Figure 3A). The NOP2/NSUN1 C459A mutation causes irreversible covalent crosslinks between the protein and target cytosine of the RNA substrate, causing the reverse transcription (RT) to terminate precisely at the polypeptide-cytosine-5 crosslink site (16). To identify NOP2/NSUN1 target sites, RT stops were mapped and m5C were assigned at the +1 site of sequencing reads. A clear enrichment of reads starting at C4447 on the 28S rRNA was observed only for the C459A mutant (Figure 3B), suggesting that this site is methylated by NOP2/NSUN1. Examination of all CLIP reads identified only one additional cross-link site at C27 of vtRNA1.2, which we found to be specific to the C459A mutant only (Figure 3C). Interestingly, C27 on vtRNA1.2 has previously been identified as an NSUN2 target site by miCLIP (16), suggesting that both NSUN2 and NOP2/NSUN1 could regulate the function of vtRNA1.2

bioRxiv preprint doi: https://doi.org/10.1101/2021.11.12.468419; this version posted November 13, 2021. The copyright holder for this preprint (which was not certified by peer review) is the author/funder. All rights reserved. No reuse allowed without permission.

through m^5C modification. Our analysis did not identify any potential methylations or cross-linked sites on snoRNAs. We found that WT NOP2/NSUN1 also bound to snoRNAs, suggesting that the interaction is likely independent of NOP2/NSUN1 methyltransferase activity.

To confirm the NOP2/NSUN1-mediated methylation sites identified by miCLIP on 28S rRNA and vtRNA1.2, we performed RNA bisulfite sequencing in cells treated with control vs. NOP2/NSUN1 siRNA. In accordance with the miCLIP data, a bisulfite-resistant cytosine resulting from C5 methylation was detected at positions C4447 of the 28S rRNA while all surrounding cytosines were efficiently deaminated to uracil (Figure 4). RNAi depletion of NOP2/NSUN1 resulted in a significant loss in bisulfite resistant (non-deaminated) cytosine at this position, confirming that NOP2/NSUN1 is the methyltransferase responsible for the deposition of m^5C at residue 4447 of the 28S rRNA (Figure 4). RNA bisulfite sequencing analysis did not find any m^5C on vtRNA1.2, which is consistent with the study of Hussain *et al.* (16) that also identified C27 on vtRNA1.2 as a NSUN2 target by miCLIP but failed to detect any m^5C by bisulfite sequencing. NSUN2-mediated m^5C of vtRNAs has been shown to positively regulate their cleavage into specific small RNAs called vtRNA-derived small RNA (svRNA) (16,59). It is possible that most of the vtRNA1.2 pool methylated at C27 is subjected to endonucleolytic processing and thus not amenable for detection by bisulfite sequencing. Further experiment will be needed to confirm whether vtRNA1.2 is a *bona fide* target of NOP2/NSUN1.

NOP2/NSUN1 is required efficient rRNA processing and 60S ribosome biogenesis

Our miCLIP analysis revealed non-crosslinked binding to the 5'ETS region of the pre-rRNA transcript and to box C/D snoRNAs for both WT and C459A mutant, suggesting that NOP2/NSUN1 has additional functions beyond catalyzing target modification. Previous CLIP studies have found that RNA-binding proteins (RBPs) enriched for C/D-box snoRNAs, which canonically guide endonucleolytic cleavage and 2'O-methylation of rRNA, also had correlated enrichment to the 5'ETS of the rRNA precursor (46,60,61). This suggests that NOP2/NSUN1 may regulate C/D-box snoRNAs-dependent processing events. To investigate this, we first performed a detailed pre-rRNA processing analysis by Northern blotting using specific probes designed to detect most of the major pre-rRNA intermediates (Figure 5A). We find that depletion of NOP2/NSUN1 severely affected the maturation steps leading to the formation of the 5.8S and 28S rRNAs from the 60S sub-unit, as observed by a marked reduction in 32S and 12S intermediates (Figure 5B-C and Supplementary Figure S2A). Processing of the 5'ETS was also compromised as evidenced by the modest but consistent increase of the 47S, 45S and 41S transcripts, indicating inefficient cleavage at sites A', A0 and 1 (Figure 5B-C and Supplementary Figure S2A). Accumulation of the 34S precursor transcript was also observed, indicating processing delays in the ITS1 region as well (Figure 5B-C and Supplementary Figure S2A). Together our findings suggests that, in addition to methylating the 28S rRNA at position C4447, NOP2/NSUN1 appears to be important for multiple steps of rRNA processing. These NOP2/NSUN1 functions are likely linked to its binding to 5'ETS regions and U3 and U8 snoRNAs, which are required for 5'ETS, ITS1 and ITS2 maturation (62).

bioRxiv preprint doi: https://doi.org/10.1101/2021.11.12.468419; this version posted November 13, 2021. The copyright holder for this preprint (which was not certified by peer review) is the author/funder. All rights reserved. No reuse allowed without permission.

Although steady state levels of mature rRNAs (5S, 5.8S, 18S and 28S) remained unaffected by NOP2/NSUN1 depletion (Figure 5B and Supplementary Figure S2B-C), the strong ITS2 rRNA processing defects observed suggest that NOP2/NSUN1, like its yeast homolog, is essential for 60S ribosomal subunit biogenesis (63). To confirm this, we performed polysome profiling to monitor the levels of 40S and 60S subunits, 80S monosomes and polysomes produced in absence of NOP2/NSUN1. Because depletion of NOP2/NSUN1 by RNAi severely impairs cell proliferation, we established stable cell lines expressing Dox-inducible NOP2/NSUN1 shRNA. Compared with uninduced cells, cells depleted of NOP2/NSUN1 by doxycycline treatment showed specific reduction in 60S levels as evidenced by the increase in 40S to 60S ratio and consequent decline in 80S monosomes (Figure 6A-B). While the levels of polysomes were not apparently reduced by NOP2/NSUN1 depletion, puromycin labeling revealed a significant decrease in overall translation rate (Figure 6C-D). Finally, sucrose gradient fractionation of pre-ribosomes followed by Western blotting revealed that NOP2/NSUN1 specifically co-sediments with early 90S pre-ribosomal complexes, as well as pre-60S particles (Figure 6E), which is consistent with a role for NOP2/NSUN1 in regulating U3-dependent 5'ETS processing (90S complex) as well as U8-dependent cleavage reactions leading to synthesis of the large subunit rRNAs (pre-60S particle).

NOP2/NSUN1 regulates snoRNP functions

Our CLIP-seq analysis revealed that NOP2/NSUN1 likely forms a non-catalytic complex with box C/D snoRNAs, which we independently confirmed by NOP2/NSUN1 immunoprecipitation combined with qRT-PCR analysis (Supplementary Figure S1). The majority of box C/D snoRNAs guide RNA 2'-O methylation but a few of them, like U3 and U8 regulate folding and cleavage reactions leading to synthesis of the small and large subunit rRNAs, respectively (62,64,65). U3 depletion was shown to impair processing of the 5′- ETS and ITS1 regions, whereas U8 was found to primarily regulate ITS2 processing (62). These processing defects are very similar to the ones we observed after depletion of NOP2/NSUN1, suggesting that NOP2/NSUN1 may be important for the regulation the rRNA processing-related functions of U3 and U8 snoRNAs. U3 and U8 also contain the conserved box C/D motif which is recognized by 15.5K, NOP56, NOP58, and Fibrillarin; the four core proteins that together with the snoRNAs assemble to form rRNA processing snoRNPs (66). To investigate the roles of NOP2/NSUN1 in box C/D snoRNAs regulation, we first tested whether NOP2/NSUN1 associates with NOP56 and Fibrillarin by co-immunoprecipitation experiments. All commercially available NOP2/NSUN1 antibodies tested were unable to precipitate any detectable NOP2/NSUN1 proteins so we used a FLAG-tagged version to perform the interaction assay. As shown in Figure 7A, ectopically expressed FLAG-NOP2/NSUN1 co-precipitated with both NOP56 and Fibrillarin. Reversely, immunoprecipitation of NOP56 also co-precipitated NOP2/NSUN1, indicating that these proteins form a complex at endogenous level (Figure 7B). We next tested whether NOP2/NSUN1 is required for snoRNPs complex formation. Depletion of NOP2/NSUN1 by RNAi did not affect Nop56 and Fibrillarin protein levels nor the ability of NOP56 to interact with Fibrillarin as detected by co-immunoprecipitation and Western blotting experiments (Figure 7C). However, we observed a marked decrease in the level of snoRNAs, particularly U8, bound to NOP56 after knockdown of NOP2/NSUN1 (Figure

bioRxiv preprint doi: https://doi.org/10.1101/2021.11.12.468419; this version posted November 13, 2021. The copyright holder for this preprint (which was not certified by peer review) is the author/funder. All rights reserved. No reuse allowed without permission.

7D-E). Steady state levels of snoRNAs were also not affected by NOP2/NSUN1 depletion (Supplementary Figure S2B-C), suggesting that NOP2/NSUN1 is likely required for stable snoRNPs complex formation.

Inhibition of any steps of ribosome biogenesis is known to induce a nucleolar stress characterized by activation of p53 and subsequent cell cycle arrest (67-80). As previously reported, depletion of NOP2/NSUN1 by RNAi caused inhibition of cell proliferation and ribosomal stress as evidenced by stabilization of p53 and activation of its transcriptional target $p21^{CIP1}$ (Supplementary Figure S3) (81,82). However, we find that NOP2/NSUN1 knockdown also impaired cell proliferation and compromised 5'ETS and ITS2 maturation in p53-null cells (HCT116 p53 -/-) (Supplementary Figure S3). Together, our observations indicate that the rRNA processing defects observed are due to a loss of NOP2/NSUN1-dependent regulation of snoRNPs complex formation and 28S rRNA C4447 methylation and not caused by p53 activation.

DISCUSSION

In this study we used a genome-wide approach to identify RNA methylation targets of human NOP2/NSUN1 to better define its role in ribosome biogenesis. We adapted an miCLIP approach using a catalytic mutant of NOP2/NSUN1 that allowed the purification of covalently cross-linked NOP2/NSUN1 to its methylated cytosine on substrate RNA. Our findings reveal multiple roles played by NOP2/NSUN1 in the regulation of ribosome biogenesis. One function involves the deposition of m^5C at position C4447 of the 28S rRNA, which likely serve to stabilize rRNA structure and contribute to efficient ITS2 processing and large subunit assembly. Our work also uncovered an unexpected function of NOP2/NSUN1 in box C/D snoRNPs regulation that is independent of its catalytic activity, and most likely explain the complex rRNA processing defects resulting from NOP2/NSUN1 depletion.

Several studies have suggested that NOP2/NSUN1 performs additional functions independent of its C5 cytosine methylation activity (13,36). In budding yeast, the lethality of NOP2/NSUN1-deleted strain can be rescued by re-expression of a methyltransferase-dead mutant, indicating that the catalytic function of NOP2/NSUN1 is not essential for viability (36). In like manner, knockout of NOP2/NSUN1 is lethal in worms whereas mutant worms expressing a catalytically-dead NOP2/NSUN1 remain viable (13). Our findings suggest that box C/D snoRNPs regulation is an important non-catalytic function of NOP2/NSUN1 that likely contributes to the lethality phenotype of NOP2/NSUN1 depletion. In contrast to budding yeast, in which the 35S and 27S pre-rRNA transcripts accumulate in absence of NOP2/NSUN1 (63), depletion of NOP2/NSUN1 in human cells leads to a more severe rRNA processing defect marked by the accumulation of the 47S primary transcript and a distinct reduction of both 32S and 12S rRNA precursors (Figure 5). Processing of ITS1 regions was also slightly affected. These rRNA processing defects are highly similar to those observed with depletion of the U3 and U8 box C/D snoRNAs (62), which complex formation with Nop56 was impaired in the absence of NOP2/NSUN1 (Figure 7E). U8 is a vertebrate-specific snoRNA that was shown to be required for ITS2

bioRxiv preprint doi: https://doi.org/10.1101/2021.11.12.468419; this version posted November 13, 2021. The copyright holder for this preprint (which was not certified by peer review) is the author/funder. All rights reserved. No reuse allowed without permission.

maturation and the synthesis of the 5.8S and 28S rRNAs in xenopus (83,84), mouse (85) and human (62) cells. Although the mechanism is not clear, it has been proposed that U8 snoRNPs chaperone the formation of an ITS2 proximal stem required for proper processing (85). In yeast, ITS2 has been modeled to form distinct secondary structures that could independently facilitate processing events in absence of U8 (86). The difference in U8 requirement for ITS2 maturation in vertebrate may explain the more severe processing defects we observed with NOP2/NSUN1 depletion. As our data indicate that NOP2/NSUN1 is required for U8 snoRNP formation, we speculate that the decline in 32S and 12S pre-rRNAs observed with NOP2/NSUN1 or U8 knockdown is due to improperly folded ITS2-containing precursors that could be processed for degradation. Our miCLIP analysis also revealed that NOP2/NSUN1 binds to a broad range of box C/D snoRNAs involved in guiding Fibrillarin-catalyzed 2'-O-methylation on 18S and 28S rRNAs. We are currently investigating whether depletion of NOP2/NSUN1 affects their assembly into snoRNPs and if this impairs rRNA 2'-O-methylation, which could also contribute to the complex processing defects observed.

NOP2/NSUN1 has been shown to be a component of the human UTP-B complex, a stable subcomplex of 90S assembly factors, that also includes UTP-A, UTP-C and U3 snoRNP (87,88). Although its functions are not completely understood in human, yeast UTP-B is likely acting as an RNA chaperone critical to initiate the assembly of the 90S pre-ribosomal particle and depletion of some of its component has been shown to impair U3 snoRNP recruitment and processing of the pre-rRNA 5'ETS (89-93). Our CLIP analysis revealed that NOP2/NSUN1 binds to both the 5'ETS region and U3 snoRNA (Figure 3A-B), which supports a role for NOP2/NSUN1 as a UTP-B complex component and explains the accumulation of unprocessed 47S/45S primary transcript observed upon NOP2/NSUN1 knockdown. Although we found that NOP2/NSUN1 binds broadly over the entire 5'ETS with some peaks overlapping with U3 snoRNA 5' hinge binding site, most of the CLIP peaks were enriched between the A0 and 1 cleavage sites of the 5'ETS (93). In contrast, other UTP-B factors such as UTP1/PWP2, UTP12/WDR3 and UTP18 have been shown to make contact on the 5'ETS upstream of the A0 site (46,93). As U3 snoRNA-5′ETS base-pairing is thought to be facilitated by the UTP-B complex (89,90,93), we speculate that NOP2/NSUN1 could have a dual role in stabilizing the 5′ ETS regions downstream of the A0 site while facilitating the recruitment of U3 snoRNP and UTP-B for effective rRNA processing and ribosome assembly. It remains to be determined whether NOP2/NSUN1 is required for the assembly of the UTP-B complex or its recruitment to the pre-90S particle.

Recent studies in *C. elegans* have suggested that NOP2/NSUN1 is responsible for catalyzing the second known m^5C at position C2982 of the 26S rRNA (equivalent of C4447 on human 28S rRNA) (41). Soma-specific RNAi depletion of NOP2/NSUN1 reduced worm body size, impaired fecundity, gonad maturation while extending lifespan. Surprisingly, rRNA processing, 60S ribosome biogenesis and global protein synthesis were not found to be impaired by NOP2/NSUN1 depletion. Instead, changes in the translation pattern of specific mRNAs were observed, suggesting that NOP2/NSUN1 could play a role in modulating ribosome function (41). In contrast to these observations, our data demonstrate that human NOP2/NSUN1 is essential for proliferation, rRNA

bioRxiv preprint doi: https://doi.org/10.1101/2021.11.12.468419; this version posted November 13, 2021. The copyright holder for this preprint (which was not certified by peer review) is the author/funder. All rights reserved. No reuse allowed without permission.

processing and ribosome biogenesis. In line with an essential role for NOP2/NSUN1, our attempts to generate CRISPR knockouts were not successful and the only clones that could be recovered were NOP2/NSUN1 mutant heterozygotes alleles or homozygous mutants with destabilized mRNA leading to low levels of NOP2/NSUN1 protein production (not shown). NOP2/NSUN1 is found overexpressed in a broad variety of cancer and its level of expression is correlated with tumor aggressiveness, poor prognosis and therapy resistance (21,22,24-34,94). NOP2/NSUN1 depletion has been shown to suppress proliferation, migration, and invasion of colon cancer cells (94) and sensitize leukemia cells to 5-aza-cytidine treatment (95). Although inhibition of ribosome biogenesis is known to induce cell cycle arrest through p53 activation (67-80), our data demonstrate that depletion of NOP2/NSUN1 severely impairs cells proliferation in both WT and p53-null cells. Together, these observations suggest that targeted therapies aimed at interfering with NOP2/NSUN1 functions would be beneficial for a broad range of tumor type, regardless of p53 status.

DATA AVAILABILITY

The datasets generated and/or analyzed during the current study are publicly available at the GEO genomics data repository (accession # pending).

FUNDING

This work was supported by National Institutes of Health [grant number R01-CA230746 to CD].

REFERENCES

1. Boccaletto, P., Machnicka, M.A., Purta, E., Piątkowski, P., Bagiński, B., Wirecki, T.K., de Crécy-Lagard, V., Ross, R., Limbach, P.A., Kotter, A. *et al.* (2017) MODOMICS: a database of RNA modification pathways. 2017 update. *Nucleic Acids Res.*, **46**, D303-D307.
2. Liu, N., Zhou, K.I., Parisien, M., Dai, Q., Diatchenko, L. and Pan, T. (2017) N6-methyladenosine alters RNA structure to regulate binding of a low-complexity protein. *Nucleic Acids Res.*, **45**, 6051-6063.
3. Bohnsack, K.E., Höbartner, C. and Bohnsack, M.T. (2019) Eukaryotic 5-methylcytosine (m^5C) RNA Methyltransferases: Mechanisms, Cellular Functions, and Links to Disease. *Genes (Basel)*, **10**, 102.
4. Louloupi, A., Ntini, E., Conrad, T. and Ørom, U.A.V. (2018) Transient N-6-Methyladenosine Transcriptome Sequencing Reveals a Regulatory Role of m6A in Splicing Efficiency. *Cell reports*, **23**, 3429-3437.
5. Yang, X., Yang, Y., Sun, B.-F., Chen, Y.-S., Xu, J.-W., Lai, W.-Y., Li, A., Wang, X., Bhattarai, D.P., Xiao, W. *et al.* (2017) 5-methylcytosine promotes mRNA export — NSUN2 as the methyltransferase and ALYREF as an m5C reader. *Cell Res.*, **27**, 606-625.

bioRxiv preprint doi: https://doi.org/10.1101/2021.11.12.468419; this version posted November 13, 2021. The copyright holder for this preprint (which was not certified by peer review) is the author/funder. All rights reserved. No reuse allowed without permission.

6. Arguello, A.E., DeLiberto, A.N. and Kleiner, R.E. (2017) RNA Chemical Proteomics Reveals the N6-Methyladenosine (m6A)-Regulated Protein–RNA Interactome. *J. Am. Chem. Soc.*, **139**, 17249-17252.
7. Frye, M., Harada, B.T., Behm, M. and He, C. (2018) RNA modifications modulate gene expression during development. *Science*, **361**, 1346-1349.
8. Delaunay, S. and Frye, M. (2019) RNA modifications regulating cell fate in cancer. *Nat. Cell Biol.*, **21**, 552-559.
9. Winkler, R., Gillis, E., Lasman, L., Safra, M., Geula, S., Soyris, C., Nachshon, A., Tai-Schmiedel, J., Friedman, N., Le-Trilling, V.T.K. *et al.* (2019) m6A modification controls the innate immune response to infection by targeting type I interferons. *Nat. Immunol.*, **20**, 173-182.
10. Wnuk, M., Slipek, P., Dziedzic, M. and Lewinska, A. (2020) The Roles of Host 5-Methylcytosine RNA Methyltransferases during Viral Infections. *International journal of molecular sciences*, **21**, 8176.
11. Kong, W., Biswas, A., Zhou, D., Fiches, G., Fujinaga, K., Santoso, N. and Zhu, J. (2020) Nucleolar protein NOP2/NSUN1 suppresses HIV-1 transcription and promotes viral latency by competing with Tat for TAR binding and methylation. *PLoS Pathog.*, **16**, e1008430.
12. Engel, M., Eggert, C., Kaplick, P.M., Eder, M., Röh, S., Tietze, L., Namendorf, C., Arloth, J., Weber, P., Rex-Haffner, M. *et al.* (2018) The Role of m(6)A/m-RNA Methylation in Stress Response Regulation. *Neuron*, **99**, 389-403.e389.
13. Navarro, I.C., Tuorto, F., Jordan, D., Legrand, C., Price, J., Braukmann, F., Hendrick, A.G., Akay, A., Kotter, A., Helm, M. *et al.* (2021) Translational adaptation to heat stress is mediated by RNA 5-methylcytosine in Caenorhabditis elegans. *EMBO J.*, **40**, e105496.
14. Heissenberger, C., Liendl, L., Nagelreiter, F., Gonskikh, Y., Yang, G., Stelzer, E.M., Krammer, T.L., Micutkova, L., Vogt, S., Kreil, D.P. *et al.* (2019) Loss of the ribosomal RNA methyltransferase NSUN5 impairs global protein synthesis and normal growth. *Nucleic Acids Res.*, **47**, 11807-11825.
15. Haag, S., Warda, A.S., Kretschmer, J., Günnigmann, M.A., Höbartner, C. and Bohnsack, M.T. (2015) NSUN6 is a human RNA methyltransferase that catalyzes formation of m5C72 in specific tRNAs. *RNA*, **21**, 1532-1543.
16. Hussain, S., Sajini, Abdulrahim A., Blanco, S., Dietmann, S., Lombard, P., Sugimoto, Y., Paramor, M., Gleeson, Joseph G., Odom, Duncan T., Ule, J. *et al.* (2013) NSun2-Mediated Cytosine-5 Methylation of Vault Noncoding RNA Determines Its Processing into Regulatory Small RNAs. *Cell reports*, **4**, 255-261.
17. Squires, J.E., Patel, H.R., Nousch, M., Sibbritt, T., Humphreys, D.T., Parker, B.J., Suter, C.M. and Preiss, T. (2012) Widespread occurrence of 5-methylcytosine in human coding and non-coding RNA. *Nucleic Acids Res.*, **40**, 5023-5033.
18. Metodiev, M.D., Spåhr, H., Loguercio Polosa, P., Meharg, C., Becker, C., Altmueller, J., Habermann, B., Larsson, N.G. and Ruzzenente, B. (2014) NSUN4 is a dual function mitochondrial protein required for both methylation of 12S rRNA and coordination of mitoribosomal assembly. *PLoS Genet.*, **10**, e1004110.
19. Nakano, S., Suzuki, T., Kawarada, L., Iwata, H., Asano, K. and Suzuki, T. (2016) NSUN3 methylase initiates 5-formylcytidine biogenesis in human mitochondrial tRNA(Met). *Nat. Chem. Biol.*, **12**, 546-551.

bioRxiv preprint doi: https://doi.org/10.1101/2021.11.12.468419; this version posted November 13, 2021. The copyright holder for this preprint (which was not certified by peer review) is the author/funder. All rights reserved. No reuse allowed without permission.

20. Khan, M.A., Rafiq, M.A., Noor, A., Hussain, S., Flores, J.V., Rupp, V., Vincent, A.K., Malli, R., Ali, G., Khan, F.S. *et al.* (2012) Mutation in NSUN2, which encodes an RNA methyltransferase, causes autosomal-recessive intellectual disability. *Am. J. Hum. Genet.*, **90**, 856-863.
21. McGrath, P.C., Holley, D.T., Hamby, L.S., Mattingly, C.A. and Freeman, J.W. (1994) Prospective study correlating P120 antigen expression with established prognostic factors in breast cancer. *Surg. Oncol.*, **3**, 69-77.
22. Fonagy, A., Swiderski, C., Ostrovsky, A.M., Bolton, W.E. and Freeman, J.W. (1994) Effect of nucleolar P120 expression level on the proliferation capacity of breast cancer cells. *Cancer Res.*, **54**, 1859-1864.
23. Janin, M., Ortiz-Barahona, V., de Moura, M.C., Martínez-Cardús, A., Llinàs-Arias, P., Soler, M., Nachmani, D., Pelletier, J., Schumann, U., Calleja-Cervantes, M.E. *et al.* (2019) Epigenetic loss of RNA-methyltransferase NSUN5 in glioma targets ribosomes to drive a stress adaptive translational program. *Acta Neuropathol.*, **138**, 1053-1074.
24. Freeman, J.W., McGrath, P., Bondada, V., Selliah, N., Ownby, H., Maloney, T., Busch, R.K. and Busch, H. (1991) Prognostic significance of proliferation associated nucleolar antigen P120 in human breast carcinoma. *Cancer Res.*, **51**, 1973-1978.
25. Gorczyca, W., Bruno, S., Melamed, M.R. and Darzynkiewicz, Z. (1992) Cell cycle-related expression of p120 nucleolar antigen in normal human lymphocytes and in cells of HL-60 and MOLT-4 leukemic lines: effects of methotrexate, camptothecin, and teniposide. *Cancer Res.*, **52**, 3491-3494.
26. Fonagy, A., Swiderski, C., Wilson, A., Bolton, W., Kenyon, N. and Freeman, J.W. (1993) Cell cycle regulated expression of nucleolar antigen P120 in normal and transformed human fibroblasts. *J. Cell. Physiol.*, **154**, 16-27.
27. McGrath, P.C., Holley, D.T., Hamby, L.S., Powell, D.E., Mattingly, C. and Freeman, J.W. (1994) Proliferation-associated nucleolar antigen P120: a prognostic marker in node-negative breast cancer. *Surgery*, **116**, 616-620; discussion 620-611.
28. Fonagy, A., Swiderski, C. and Freeman, J.W. (1995) Altered transcription control is responsible for the increased level of proliferation-associated P120 in rapidly growing breast carcinoma. *Int. J. Cancer*, **60**, 407-412.
29. Uchiyama, B., Saijo, Y., Kumano, N., Abe, T., Fujimura, S., Ohkuda, K., Handa, M., Satoh, K. and Nukiwa, T. (1997) Expression of nucleolar protein p120 in human lung cancer: Difference in histological types as a marker for proliferation. *Clinical cancer research : an official journal of the American Association for Cancer Research*, **3**, 1873-1877.
30. Ueki, T., Nakayama, Y., Sugao, Y., Kohno, K., Matsuo, K., Sugimoto, Y., Yamada, Y., Kuwano, M. and Tsuneyoshi, M. (1997) Significance of the expression of proliferation-associated nucleolar antigen p120 in human colorectal tumors. *Hum. Pathol.*, **28**, 74-79.
31. Sato, K., Nishi, T., Takeshima, H., Kochi, M., Kuratsu, J., Masuko, N., Sugimoto, Y., Yamada, Y. and Ushio, Y. (1999) Expression of p120 nucleolar proliferating antigen in human gliomas and growth suppression of glioma cells by p120 ribozyme vector. *Int. J. Oncol.*, **14**, 417-424.

bioRxiv preprint doi: https://doi.org/10.1101/2021.11.12.468419; this version posted November 13, 2021. The copyright holder for this preprint (which was not certified by peer review) is the author/funder. All rights reserved. No reuse allowed without permission.

32. Ventura, L., Migaldi, M., Criscuolo, M., Castelli, M., Barbolini, G., Ranieri, A., Bifaretti, G., Uboldi, P. and Leocata, P. (1999) Nucleolar protein p120 expression in oral carcinoma. *Anticancer Res.*, **19**, 1423-1426.
33. Trerè, D., Migaldi, M., Montanaro, L., Pession, A. and Derenzini, M. (2000) p120 expression provides a reliable indication of the rapidity of cell duplication in cancer cells independently of tumour origin. *J. Pathol.*, **192**, 216-220.
34. Saijo, Y., Sato, G., Usui, K., Sato, M., Sagawa, M., Kondo, T., Minami, Y. and Nukiwa, T. (2001) Expression of nucleolar protein p120 predicts poor prognosis in patients with stage I lung adenocarcinoma. *Ann. Oncol.*, **12**, 1121-1125.
35. Perlaky, L., Valdez, B.C., Busch, R.K., Larson, R.G., Jhiang, S.M., Zhang, W.W., Brattain, M. and Busch, H. (1992) Increased growth of NIH/3T3 cells by transfection with human p120 complementary DNA and inhibition by a p120 antisense construct. *Cancer Res.*, **52**, 428-436.
36. Sharma, S., Yang, J., Watzinger, P., Kötter, P. and Entian, K.D. (2013) Yeast Nop2 and Rcm1 methylate C2870 and C2278 of the 25S rRNA, respectively. *Nucleic Acids Res.*, **41**, 9062-9076.
37. Song, Q., Qiu, Z., Wang, H., Xia, Y., Shen, J. and Zhang, Y. (2013) The effect of methylation on the hydrogen-bonding and stacking interaction of nucleic acid bases. *Struct. Chem.*, **24**, 55-65.
38. Taoka, M., Nobe, Y., Yamaki, Y., Sato, K., Ishikawa, H., Izumikawa, K., Yamauchi, Y., Hirota, K., Nakayama, H., Takahashi, N. *et al.* (2018) Landscape of the complete RNA chemical modifications in the human 80S ribosome. *Nucleic Acids Res.*, **46**, 9289-9298.
39. Natchiar, S.K., Myasnikov, A.G., Kratzat, H., Hazemann, I. and Klaholz, B.P. (2017) Visualization of chemical modifications in the human 80S ribosome structure. *Nature*, **551**, 472-477.
40. Bourgeois, G., Ney, M., Gaspar, I., Aigueperse, C., Schaefer, M., Kellner, S., Helm, M. and Motorin, Y. (2015) Eukaryotic rRNA Modification by Yeast 5-Methylcytosine-Methyltransferases and Human Proliferation-Associated Antigen p120. *PLoS One*, **10**, e0133321.
41. Heissenberger, C., Rollins, J.A., Krammer, T.L., Nagelreiter, F., Stocker, I., Wacheul, L., Shpylovyi, A., Tav, K., Snow, S., Grillari, J. *et al.* (2020) The ribosomal RNA m(5)C methyltransferase NSUN-1 modulates healthspan and oogenesis in Caenorhabditis elegans. *eLife*, **9**, e56205.
42. Wiederschain, D., Wee, S., Chen, L., Loo, A., Yang, G., Huang, A., Chen, Y., Caponigro, G., Yao, Y.M., Lengauer, C. *et al.* (2009) Single-vector inducible lentiviral RNAi system for oncology target validation. *Cell cycle (Georgetown, Tex.)*, **8**, 498-504.
43. Tiscornia, G., Singer, O. and Verma, I.M. (2006) Production and purification of lentiviral vectors. *Nat. Protoc.*, **1**, 241-245.
44. Simsek, D., Tiu, G.C., Flynn, R.A., Byeon, G.W., Leppek, K., Xu, A.F., Chang, H.Y. and Barna, M. (2017) The Mammalian Ribo-interactome Reveals Ribosome Functional Diversity and Heterogeneity. *Cell*, **169**, 1051-1065.e1018.
45. Pestov, D.G., Lapik, Y.R. and Lau, L.F. (2008) Assays for ribosomal RNA processing and ribosome assembly. *Curr. Protoc. Cell Biol.*, **Chapter 22**, Unit 22 11.

bioRxiv preprint doi: https://doi.org/10.1101/2021.11.12.468419; this version posted November 13, 2021. The copyright holder for this preprint (which was not certified by peer review) is the author/funder. All rights reserved. No reuse allowed without permission.

46. Van Nostrand, E.L., Pratt, G.A., Yee, B.A., Wheeler, E.C., Blue, S.M., Mueller, J., Park, S.S., Garcia, K.E., Gelboin-Burkhart, C., Nguyen, T.B. *et al.* (2020) Principles of RNA processing from analysis of enhanced CLIP maps for 150 RNA binding proteins. *Genome Biol.*, **21**, 90.
47. Van Nostrand, E.L., Nguyen, T.B., Gelboin-Burkhart, C., Wang, R., Blue, S.M., Pratt, G.A., Louie, A.L. and Yeo, G.W. (2017) Robust, Cost-Effective Profiling of RNA Binding Protein Targets with Single-end Enhanced Crosslinking and Immunoprecipitation (seCLIP). *Methods Mol. Biol.*, **1648**, 177-200.
48. Martin, M. (2011) Cutadapt removes adapter sequences from high-throughput sequencing reads. *2011*, **17**, 3.
49. Chen, S., Zhou, Y., Chen, Y. and Gu, J. (2018) fastp: an ultra-fast all-in-one FASTQ preprocessor. *Bioinformatics*, **34**, i884-i890.
50. Langmead, B. and Salzberg, S.L. (2012) Fast gapped-read alignment with Bowtie 2. *Nat. Methods*, **9**, 357-359.
51. Smith, T., Heger, A. and Sudbery, I. (2017) UMI-tools: modeling sequencing errors in Unique Molecular Identifiers to improve quantification accuracy. *Genome Res.*, **27**, 491-499.
52. Li, H. (2011) A statistical framework for SNP calling, mutation discovery, association mapping and population genetical parameter estimation from sequencing data. *Bioinformatics*, **27**, 2987-2993.
53. King, M.Y. and Redman, K.L. (2002) RNA methyltransferases utilize two cysteine residues in the formation of 5-methylcytosine. *Biochemistry*, **41**, 11218-11225.
54. Liu, R.J., Long, T., Li, J., Li, H. and Wang, E.D. (2017) Structural basis for substrate binding and catalytic mechanism of a human RNA:m5C methyltransferase NSun6. *Nucleic Acids Res.*, **45**, 6684-6697.
55. Van Nostrand, E.L., Pratt, G.A., Shishkin, A.A., Gelboin-Burkhart, C., Fang, M.Y., Sundararaman, B., Blue, S.M., Nguyen, T.B., Surka, C., Elkins, K. *et al.* (2016) Robust transcriptome-wide discovery of RNA-binding protein binding sites with enhanced CLIP (eCLIP). *Nat. Methods*, **13**, 508-514.
56. Drygin, D., Rice, W.G. and Grummt, I. (2010) The RNA polymerase I transcription machinery: an emerging target for the treatment of cancer. *Annu. Rev. Pharmacol. Toxicol.*, **50**, 131-156.
57. Goodfellow, S.J. and Zomerdijk, J.C. (2013) Basic mechanisms in RNA polymerase I transcription of the ribosomal RNA genes. *Subcell. Biochem.*, **61**, 211-236.
58. Ciganda, M. and Williams, N. (2011) Eukaryotic 5S rRNA biogenesis. *Wiley interdisciplinary reviews. RNA*, **2**, 523-533.
59. Sajini, A.A., Choudhury, N.R., Wagner, R.E., Bornelöv, S., Selmi, T., Spanos, C., Dietmann, S., Rappsilber, J., Michlewski, G. and Frye, M. (2019) Loss of 5-methylcytosine alters the biogenesis of vault-derived small RNAs to coordinate epidermal differentiation. *Nature communications*, **10**, 2550.
60. Kaiser, R.W.J., Ignarski, M., Van Nostrand, E.L., Frese, C.K., Jain, M., Cukoski, S., Heinen, H., Schaechter, M., Seufert, L., Bunte, K. *et al.* (2019) A protein-RNA interaction atlas of the ribosome biogenesis factor AATF. *Sci. Rep.*, **9**, 11071.

bioRxiv preprint doi: https://doi.org/10.1101/2021.11.12.468419; this version posted November 13, 2021. The copyright holder for this preprint (which was not certified by peer review) is the author/funder. All rights reserved. No reuse allowed without permission.

61. Calo, E., Flynn, R.A., Martin, L., Spitale, R.C., Chang, H.Y. and Wysocka, J. (2015) RNA helicase DDX21 coordinates transcription and ribosomal RNA processing. *Nature*, **518**, 249-253.
62. Langhendries, J.L., Nicolas, E., Doumont, G., Goldman, S. and Lafontaine, D.L. (2016) The human box C/D snoRNAs U3 and U8 are required for pre-rRNA processing and tumorigenesis. *Oncotarget*, **7**, 59519-59534.
63. Hong, B., Brockenbrough, J.S., Wu, P. and Aris, J.P. (1997) Nop2p is required for pre-rRNA processing and 60S ribosome subunit synthesis in yeast. *Mol. Cell. Biol.*, **17**, 378-388.
64. Terns, M.P. and Terns, R.M. (2002) Small nucleolar RNAs: versatile trans-acting molecules of ancient evolutionary origin. *Gene Expr.*, **10**, 17-39.
65. Watkins, N.J., Lemm, I. and Lührmann, R. (2007) Involvement of nuclear import and export factors in U8 box C/D snoRNP biogenesis. *Mol. Cell. Biol.*, **27**, 7018-7027.
66. Watkins, N.J., Lemm, I., Ingelfinger, D., Schneider, C., Hoßbach, M., Urlaub, H. and Lührmann, R. (2004) Assembly and Maturation of the U3 snoRNP in the Nucleoplasm in a Large Dynamic Multiprotein Complex. *Mol. Cell*, **16**, 789-798.
67. Pestov, D.G., Strezoska, Z. and Lau, L.F. (2001) Evidence of p53-dependent cross-talk between ribosome biogenesis and the cell cycle: effects of nucleolar protein Bop1 on G(1)/S transition. *Mol. Cell. Biol.*, **21**, 4246-4255.
68. Lohrum, M.A., Ludwig, R.L., Kubbutat, M.H., Hanlon, M. and Vousden, K.H. (2003) Regulation of HDM2 activity by the ribosomal protein L11. *Cancer Cell*, **3**, 577-587.
69. Rubbi, C.P. and Milner, J. (2003) Disruption of the nucleolus mediates stabilization of p53 in response to DNA damage and other stresses. *EMBO J.*, **22**, 6068-6077.
70. Zhang, Y., Wolf, G.W., Bhat, K., Jin, A., Allio, T., Burkhart, W.A. and Xiong, Y. (2003) Ribosomal protein L11 negatively regulates oncoprotein MDM2 and mediates a p53-dependent ribosomal-stress checkpoint pathway. *Mol. Cell. Biol.*, **23**, 8902-8912.
71. Bhat, K.P., Itahana, K., Jin, A. and Zhang, Y. (2004) Essential role of ribosomal protein L11 in mediating growth inhibition-induced p53 activation. *EMBO J.*, **23**, 2402-2412.
72. Dai, M.S. and Lu, H. (2004) Inhibition of MDM2-mediated p53 ubiquitination and degradation by ribosomal protein L5. *J. Biol. Chem.*, **279**, 44475-44482.
73. Dai, M.S., Zeng, S.X., Jin, Y., Sun, X.X., David, L. and Lu, H. (2004) Ribosomal protein L23 activates p53 by inhibiting MDM2 function in response to ribosomal perturbation but not to translation inhibition. *Mol. Cell. Biol.*, **24**, 7654-7668.
74. Jin, A., Itahana, K., O'Keefe, K. and Zhang, Y. (2004) Inhibition of HDM2 and activation of p53 by ribosomal protein L23. *Mol. Cell. Biol.*, **24**, 7669-7680.
75. Yuan, X., Zhou, Y., Casanova, E., Chai, M., Kiss, E., Grone, H.J., Schutz, G. and Grummt, I. (2005) Genetic inactivation of the transcription factor TIF-IA leads to nucleolar disruption, cell cycle arrest, and p53-mediated apoptosis. *Mol. Cell*, **19**, 77-87.
76. Chen, D., Zhang, Z., Li, M., Wang, W., Li, Y., Rayburn, E.R., Hill, D.L., Wang, H. and Zhang, R. (2007) Ribosomal protein S7 as a novel modulator of p53-MDM2

bioRxiv preprint doi: https://doi.org/10.1101/2021.11.12.468419; this version posted November 13, 2021. The copyright holder for this preprint (which was not certified by peer review) is the author/funder. All rights reserved. No reuse allowed without permission.

interaction: binding to MDM2, stabilization of p53 protein, and activation of p53 function. *Oncogene*, **26**, 5029-5037.

77. Fumagalli, S., Di Cara, A., Neb-Gulati, A., Natt, F., Schwemberger, S., Hall, J., Babcock, G.F., Bernardi, R., Pandolfi, P.P. and Thomas, G. (2009) Absence of nucleolar disruption after impairment of 40S ribosome biogenesis reveals an rpL11-translation-dependent mechanism of p53 induction. *Nat. Cell Biol.*, **11**, 501-508.
78. Zhu, Y., Poyurovsky, M.V., Li, Y., Biderman, L., Stahl, J., Jacq, X. and Prives, C. (2009) Ribosomal protein S7 is both a regulator and a substrate of MDM2. *Mol. Cell*, **35**, 316-326.
79. Holzel, M., Orban, M., Hochstatter, J., Rohrmoser, M., Harasim, T., Malamoussi, A., Kremmer, E., Langst, G. and Eick, D. (2010) Defects in 18 S or 28 S rRNA processing activate the p53 pathway. *J. Biol. Chem.*, **285**, 6364-6370.
80. Golomb, L., Volarevic, S. and Oren, M. (2014) p53 and ribosome biogenesis stress: The essentials. *FEBS Lett.*, **588**, 2571-2579.
81. Sloan, K.E., Bohnsack, M.T. and Watkins, N.J. (2013) The 5S RNP couples p53 homeostasis to ribosome biogenesis and nucleolar stress. *Cell reports*, **5**, 237-247.
82. Liao, H., Gaur, A., Mauvais, C. and Denicourt, C. (2021) p53 induces a survival transcriptional response after nucleolar stress. *Mol. Biol. Cell*, **32**, ar3.
83. Peculis, B.A. and Steitz, J.A. (1993) Disruption of U8 nucleolar snRNA inhibits 5.8S and 28S rRNA processing in the Xenopus oocyte. *Cell*, **73**, 1233-1245.
84. Peculis, B.A. (1997) The sequence of the 5' end of the U8 small nucleolar RNA is critical for 5.8S and 28S rRNA maturation. *Mol. Cell. Biol.*, **17**, 3702-3713.
85. Michot, B., Joseph, N., Mazan, S. and Bachellerie, J.P. (1999) Evolutionarily conserved structural features in the ITS2 of mammalian pre-rRNAs and potential interactions with the snoRNA U8 detected by comparative analysis of new mouse sequences. *Nucleic Acids Res.*, **27**, 2271-2282.
86. Côté, C.A., Greer, C.L. and Peculis, B.A. (2002) Dynamic conformational model for the role of ITS2 in pre-rRNA processing in yeast. *RNA*, **8**, 786-797.
87. Sloan, K.E., Leisegang, M.S., Doebele, C., Ramírez, A.S., Simm, S., Safferthal, C., Kretschmer, J., Schorge, T., Markoutsa, S., Haag, S. *et al.* (2015) The association of late-acting snoRNPs with human pre-ribosomal complexes requires the RNA helicase DDX21. *Nucleic Acids Res.*, **43**, 553-564.
88. Bohnsack, K.E. and Bohnsack, M.T. (2019) Uncovering the assembly pathway of human ribosomes and its emerging links to disease. *EMBO J.*, **38**, e100278.
89. Hunziker, M., Barandun, J., Petfalski, E., Tan, D., Delan-Forino, C., Molloy, K.R., Kim, K.H., Dunn-Davies, H., Shi, Y., Chaker-Margot, M. *et al.* (2016) UtpA and UtpB chaperone nascent pre-ribosomal RNA and U3 snoRNA to initiate eukaryotic ribosome assembly. *Nature communications*, **7**, 12090.
90. Dosil, M. and Bustelo, X.R. (2004) Functional characterization of Pwp2, a WD family protein essential for the assembly of the 90 S pre-ribosomal particle. *J. Biol. Chem.*, **279**, 37385-37397.
91. Sloan, K.E., Bohnsack, M.T., Schneider, C. and Watkins, N.J. (2014) The roles of SSU processome components and surveillance factors in the initial processing of human ribosomal RNA. *RNA*, **20**, 540-550.

bioRxiv preprint doi: https://doi.org/10.1101/2021.11.12.468419; this version posted November 13, 2021. The copyright holder for this preprint (which was not certified by peer review) is the author/funder. All rights reserved. No reuse allowed without permission.

92. Mullineux, S.T. and Lafontaine, D.L. (2012) Mapping the cleavage sites on mammalian pre-rRNAs: where do we stand? *Biochimie*, **94**, 1521-1532.
93. Singh, S., Broeck, A.V., Miller, L., Chaker-Margot, M. and Klinge, S. (2021) Nucleolar maturation of the human small subunit processome. *Science*, **373**, eabj5338.
94. Bi, J., Huang, Y. and Liu, Y. (2019) Effect of NOP2 knockdown on colon cancer cell proliferation, migration, and invasion. *Translational Cancer Research*, **8**, 2274-2283.
95. Cheng, J.X., Chen, L., Li, Y., Cloe, A., Yue, M., Wei, J., Watanabe, K.A., Shammo, J.M., Anastasi, J., Shen, Q.J. *et al.* (2018) RNA cytosine methylation and methyltransferases mediate chromatin organization and 5-azacytidine response and resistance in leukaemia. *Nature communications*, **9**, 1163.
96. Lu, Z., Zhang, Q.C., Lee, B., Flynn, R.A., Smith, M.A., Robinson, J.T., Davidovich, C., Gooding, A.R., Goodrich, K.J., Mattick, J.S. *et al.* (2016) RNA Duplex Map in Living Cells Reveals Higher-Order Transcriptome Structure. *Cell*, **165**, 1267-1279.

Table and Figure Legends

Figure 1. Human NOP2/NSUN1 miCLIP design. **(A)** Alignment of the protein sequences of human NSUN family members showing conserved cysteine residues (highlighted) required for catalytic activity. The mutated cysteine in motif IV used for the miCLIP is indicated as C459 **(B)** Cartoon showing that only NOP2/NUSN1 C459A mutant forms irreversible covalent crosslinks with its RNA substrate. **(C)** FLAG-tagged NOP2/NSUN1 Wildtype and C459A mutant were immunoprecipitated with a FLAG antibody and immunoblotted with FLAG antibody. **(D)** FLAG-tagged NOP2/NSUN1 Wildtype and C459A mutant were immunoprecipitated by FLAG antibody and 3'-end labeled with pCp-biotin for detection of co-precipitated RNA. After membrane transfer, the pCp-biotin labeled RNA was detected with Streptavidin-IR800. Immunoprecipitated NOP2/NSUN1 Wildtype and C459A mutant were detected by immunoblotting with a FLAG antibody. Right panel show a high exposure of the pCp-biotin labeled RNA with relative densitometry analysis. **(E)** Schematic overview of NOP2/NSUN1 miCLIP-sequencing. Cells were lysed, digested with RNase, immunoprecipitated with FLAG antibody, separated on SDS-PAGE gel and transferred to membrane. NOP2/NSUN1 Wildtype and C459A mutant associated RNAs as well as their respective size matched inputs (SMInputs) were extracted from the membrane and processed for sequencing libraries.

Figure 2. Human NOP2/NSUN1 binds to rRNA, snoRNAs, and vtRNA1.2. **(A-C)** HEK293T cells expressing FLAG-tagged NOP2/NSUN1 WT (no covalent binding to substrate) or C459A mutant (covalent binding to substrate) were subject to CLIP-sequencing analysis (two biological replicates for each sample). CLIP-sequencing reads were aligned to human genome (hg38) and repetitive elements families. CLIP peaks were called by Peakachu. **(A)** The fractions of reads in IP samples mapped to CLIP peak regions with cut-offs of adjusted significance *P* values < 0.05 and fold change over size-matched input (SMinput) >= 2. **(B)** Volcano plots displaying all peaks detected by

bioRxiv preprint doi: https://doi.org/10.1101/2021.11.12.468419; this version posted November 13, 2021. The copyright holder for this preprint (which was not certified by peer review) is the author/funder. All rights reserved. No reuse allowed without permission.

Peakachu. Each dot represents a peak either enriched in IP (Log2 fold change > 0) or SMinput samples (Log2 fold change < 0). **(C)** Number of CLIP peaks with cut-offs of adjusted significant *P* values < 0.05 and fold change over SMinput >= 2 in each indicated RNA category. C/D box and H/ACA box snoRNA are shown in light and dark blue, respectively. Number of snoRNAs found in CLIP peaks / total number of snoRNAs in indicated subfamily are shown in parentheses.

Figure 3. Human NOP2/NSUN1 binds to rRNA 5'-ETS and crosslinks on 28S rRNA at position C4447 and on vtRNA1.2 at position C27. **(A-B)** miCLIP-sequencing data was aligned to human 47S pre-rRNA (NR_046235) and the mapping information was retrieved using Samtools. The location of mature 18S, 5.8S, and 28S rRNAs are marked with light blue shadow boxes above the x-axis. A', A0 and 1 cleavage sites on 5'-ETS are marked with gray lines. Red bars beneath the x-axis indicate the location of U3 snoRNA binding sites on 47S rRNA (93). Yellow bar beneath the x-axis indicates the location of U8 snoRNA binding site on 47S rRNA (96). **(A)** Plot of sequencing depth-normalized reads ratio of IP over size-matched input (SMInput) on 47S rRNA. **(B)** Plot of reverse transcription (RT) stops on 47S rRNA normalized by sequencing depth. RT stops were assigned at the start (+1) sites of Read1 sequence. **(C)** Plot of reverse transcription (RT) stops on vtRNA1.2 normalized by sequencing depth. RT stops were assigned at the start (+1) sites of vtRNA1.2 aligned Read1 sequence of from NOP2/NSUN1 IP samples. Plotted data is represented for each independent biological replicate for NOP2/NSUN1 WT (blue lines) and C459A mutant (green lines).

Figure 4. Human NOP2/NSUN1 methylates 28S rRNA at position C4447. **(A)** HCT116 cells were transfected with non-targeting control (siC) or NOP2/NSUN1 siRNA. 72h later, NOP2/NSUN1 depletion efficiency was determined by Western blot. **(B)** A fraction of cells from (A) were harvested for nuclear RNA extraction. Nuclear RNA was converted by bisulfite salt and sequenced on Illumina Mi-Seq platform. Non-converted (indicates 5mC modification) and converted cytosines mapped to each cytosine position near C4447 were plotted. **(C)** Converted ratio of cytosine (C) at position 4447 on 28S rRNA. Data is shown as mean of 2 independent biological replicates ± standard deviation (SD). Statistical significance between NOP2/NSUN1 depleted samples and non-targeting siRNA control samples were calculated using 2-tailed independent student *t* test.

Figure 5. Human NOP2/NSUN1 is required for efficient pre-rRNA processing. **(A)** Schematic overview of human rRNA precursors and location of probes used for Northern blot. **(B)** HCT116 cells were transfected with non-targeting control (siC), NOP2 siRNA #1 or #2. After 72h, total RNA was separated on formaldehyde denaturing agarose gel and analyzed by Northern blot with 5'ETS, ITS-1, and ITS-2 probes. A fraction of cells was collected for determining NOP2 depletion efficiency by Western blot. 28S and 18S rRNA were stained by methylene blue on membrane. **(C)** Densitometry quantification of each rRNA precursor from (B) normalized to 28S rRNA. Data is presented as mean of 3 independent biological replicates ± standard deviation (SD). Statistical significance between NOP2 depleted samples and non-targeting siRNA control samples were calculated using 2-tailed independent student *t* test.

bioRxiv preprint doi: https://doi.org/10.1101/2021.11.12.468419; this version posted November 13, 2021. The copyright holder for this preprint (which was not certified by peer review) is the author/funder. All rights reserved. No reuse allowed without permission.

Figure 6. Human NOP2/NUSN1 is required for 60S ribosomal subunit biogenesis. **(A)** HCT116 cells were infected with doxycycline-inducible NOP2 shRNA expressing lentivirus. After puromycin selection, cells were induced with 200 ng/ml doxycycline (Dox+) for 4 days. Non-induced (Dox-) cells were used as control. NOP2 depletion efficiency was determined by Western blot. **(B)** A fraction of cells from (A) was analyzed by polysome profiling. Dox+ and Dox- indicates doxycycline induced and non-induced control respectively. **(C)** HCT116 cells were transfected with non-targeting control (siC) or NOP2 siRNA. 72h after transfection, cells were treated with 5 µg/ml puromycin for the indicated time. Puromycylation of nascent peptides, as well as NOP2 depletion efficiency, was determined by Western blot. **(D)** Densitometry quantification of puromycin signal of each lane from (C). Puromycin signal was normalized to corresponding GAPDH signal. Data is presented as the mean of 2 independent biological replicates ± standard deviation (SD). Statistical significance between NOP2 depleted samples and non-targeting control samples were calculated using 2-tailed independent student *t* test. **(E)** HCT116 cells were lysed and pre-ribosomal particles were separated on sucrose gradient ultra-centrifugation and fractionation. Proteins from each fraction were extracted and analyzed by Western blot with indicated antibodies.

Figure 7. NOP2/NSUN1 is required for stable U3 and U8 snoRNP formation. **(A)** HEK293T expressing empty vector (Mock) or FLAG-tagged NOP2/NUSN1 wildtype were lysed and immunoprecipitated (IP) with an anti-FLAG antibody. Associated proteins were analyzed by Western blot. Mock transfected cells were used as negative control. **(B)** NOP56 was immunoprecipitated with an anti-NOP56 antibody from HEK293T cell lysate. Associated proteins were analyzed by Western blot. Normal rabbit IgG was used as negative immunoprecipitation control. **(C)** HEK293T cells were transfected with non-targeting control (siC) or NOP2 siRNA. 72h later, cells were lysed and immunoprecipitated (IP) with an anti-NOP56 antibody. Associated proteins were analyzed by Western blot. Normal rabbit IgG was used as negative immunoprecipitation control. **(D)** HCT116 cells were transfected with non-targeting control (siC), NOP2 siRNA #1 or #2. 72h later, cells were lysed and immunoprecipitated (IP) with anti-NOP56 antibody. A fraction of associated proteins was analyzed by Western blot to control for immunoprecipitation knockdown efficiency. The remaining immunoprecipitation fraction was processed for RNA extraction. **(E)** NOP56 associated RNA from (D) was analyzed by RT-qPCR with U3 and U8 specific primers. Relative enrichment over IgG control is represented. Data is presented as mean of 3 independent biological replicates ± standard deviation (SD). Statistical significance between NOP2 depleted samples and non-targeting siRNA control samples were calculated using 2-tailed independent student *t* test.

Supplementary Figure S1. NOP2/NSUN1 binds to C/D box snoRNAs. HEK293T cells expressing FLAG-tagged NOP2/NSUN1 wildtype or C459A mutant were lysed and immunoprecipitated (IP) with an anti-FLAG antibody. Associated RNAs were analyzed by RT-qPCR. Mock transfected cells were used as negative control. Relative enrichment over Mock control is represented. Data is presented as mean of 3 independent biological replicates ± standard deviation (SD). Statistical significance between Mock and wildtype or C459A mutant IP samples was calculated using 2-tailed independent student *t* test.

bioRxiv preprint doi: https://doi.org/10.1101/2021.11.12.468419; this version posted November 13, 2021. The copyright holder for this preprint (which was not certified by peer review) is the author/funder. All rights reserved. No reuse allowed without permission.

Supplementary Figure S2. NOP2/NSUN1 depletion impairs pre-rRNA processing but has no effect on SNORD3/U3 and SNORD118/U8 stability or biogenesis. **(A)** Densitometry ratio between each two rRNA precursors on Northern blot from Figure 5B. Data is presented as mean of 3 independent biological replicates ± standard deviation (SD). Statistical significance between NOP2 depleted samples and non-targeting control samples was calculated using 2-tailed independent student *t* test. **(B)** RNA samples from Figure 5B were separated on urea-PAGE gel and analyzed by Northern blot with SNORD118/U8, SNORD3/U3, 5S, 5.8S, and 7SL specific probes. **(C)** Densitometry quantification of SNORD118/U8, SNORD3/U3, 5S, and 5.8S signal from (B) normalized to 7SL RNA signal. Data is presented as mean of 3 independent biological replicates ± standard deviation (SD). Statistical significance between NOP2 depleted samples and non-targeting control samples was calculated using 2-tailed independent student *t* test.

Supplementary Figure S3. Cell growth and pre-rRNA processing defects after NOP2/NSUN1 depletion are independent of p53 status. **(A)** HCT116 wildtype or HCT116 p53 -/- cells were transfected with non-targeting control (siC), NOP2 siRNA #1 or #2. 72h later, a fraction of cells was harvested for Western blot analysis with specific antibodies (indicated on the left of each blot). **(B)** Cells from (A) were monitored daily using MTT assay. Cell counts were normalized to non-targeting control (siC) on day 3. Data is presented as mean of 2 independent biological replicates ± standard deviation (SD). Statistical significance between NOP2 depleted samples and non-targeting control samples were calculated using 2-tailed independent student *t* test. *P<0.05 and **P<0.01: NOP2 siRNA#1 vs siC; $^{\#}$P<0.05 and $^{\#}$P<0.01: NOP2 siRNA#2 vs siC. **(C)** HCT116 p53 -/- cells were transfected with non-targeting control (siC), NOP2 siRNA #1 or #2. 72h later, total RNA was separated on formaldehyde denaturing agarose gel and analyzed by Northern blot with 5'ETS, ITS-1, and ITS-2 probes. 28S and 18S rRNA were stained by methylene blue on membrane.

Supplementary Table 1. Sequence of primers and probes used in this paper.

Supplementary Table 2. miCLIP sequencing Peaks with IP vs SMInput fold-change >= 2 and adjusted P value < 0.05.

bioRxiv preprint doi: https://doi.org/10.1101/2021.11.12.468419; this version posted November 13, 2021. The copyright holder for this preprint (which was not certified by peer review) is the author/funder. All rights reserved. No reuse allowed without permission.

Liao et al., Fig. 1

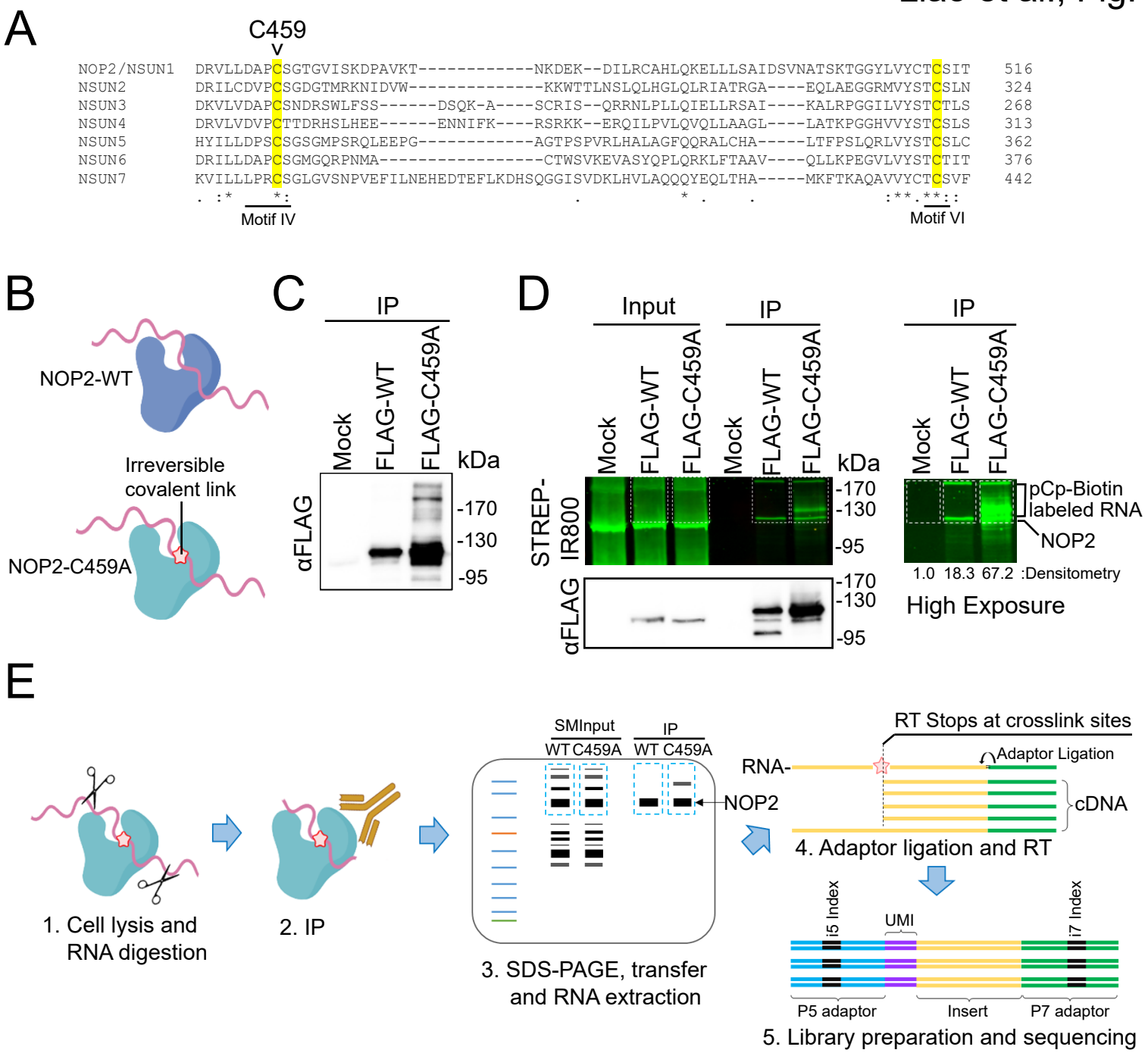

bioRxiv preprint doi: https://doi.org/10.1101/2021.11.12.468419; this version posted November 13, 2021. The copyright holder for this preprint (which was not certified by peer review) is the author/funder. All rights reserved. No reuse allowed without permission.

Liao et al., Fig. 2

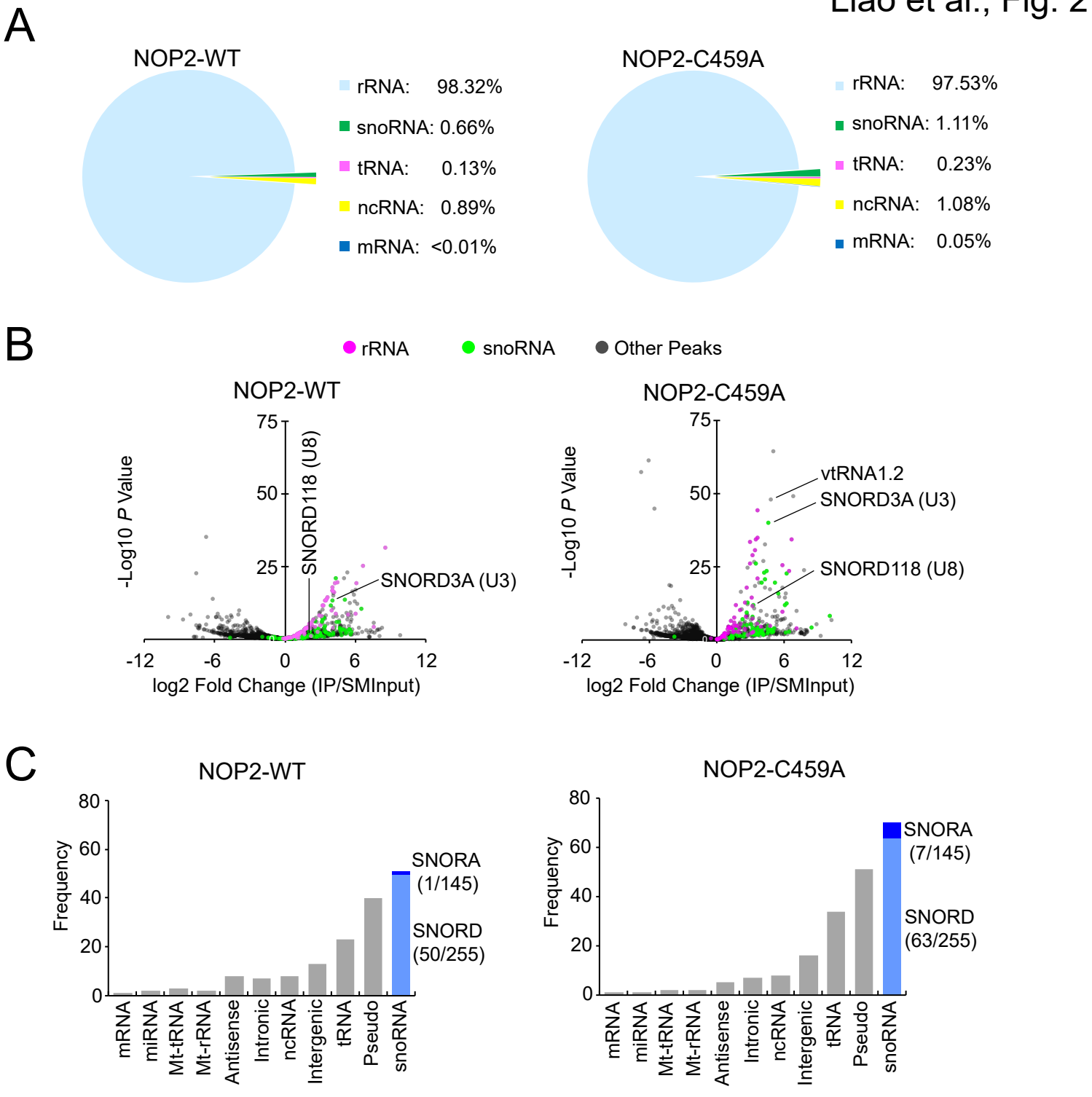

bioRxiv preprint doi: https://doi.org/10.1101/2021.11.12.468419; this version posted November 13, 2021. The copyright holder for this preprint (which was not certified by peer review) is the author/funder. All rights reserved. No reuse allowed without permission.

Liao et al., Fig. 3

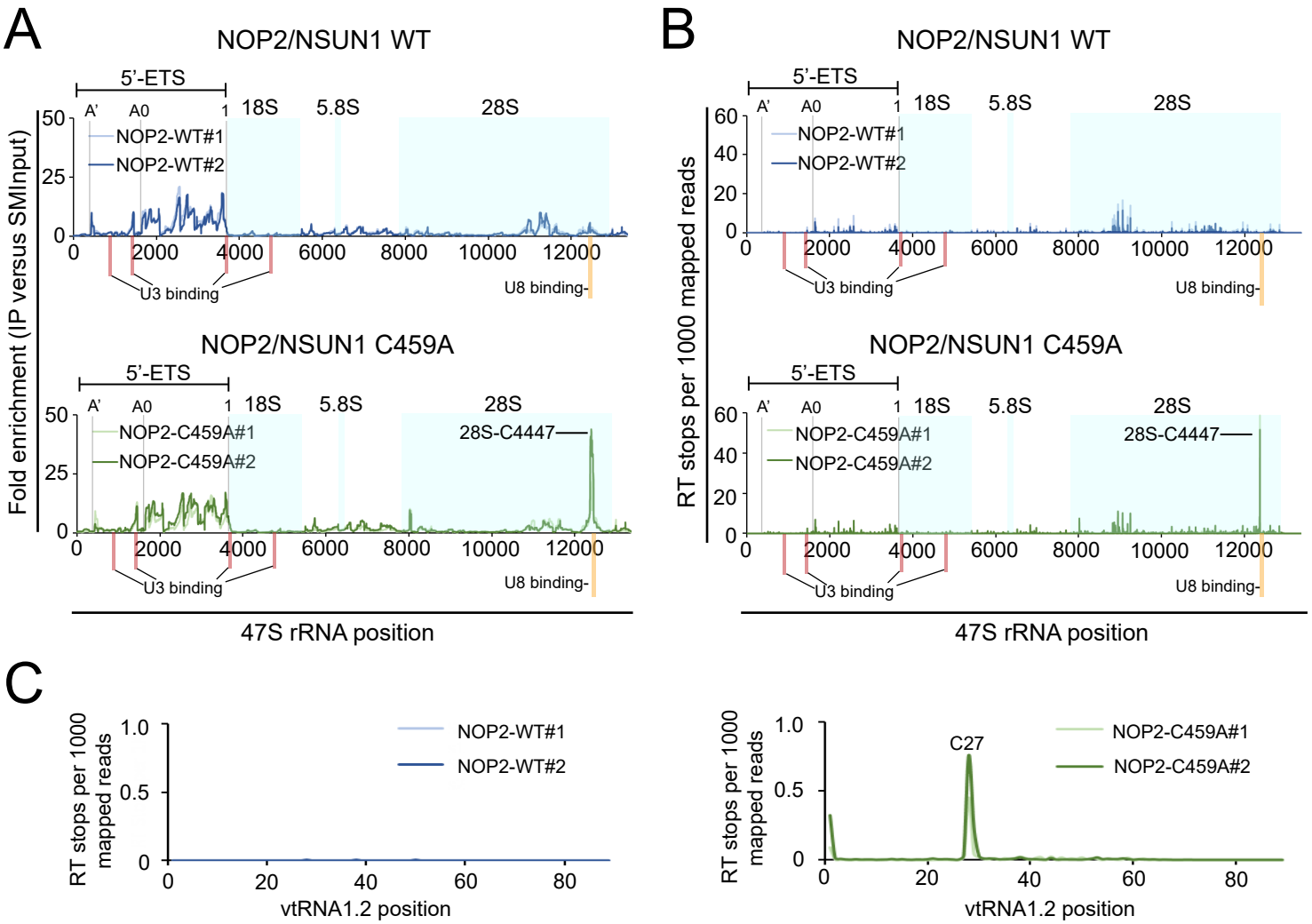

bioRxiv preprint doi: https://doi.org/10.1101/2021.11.12.468419; this version posted November 13, 2021. The copyright holder for this preprint (which was not certified by peer review) is the author/funder. All rights reserved. No reuse allowed without permission.

Liao et al., Fig. 4

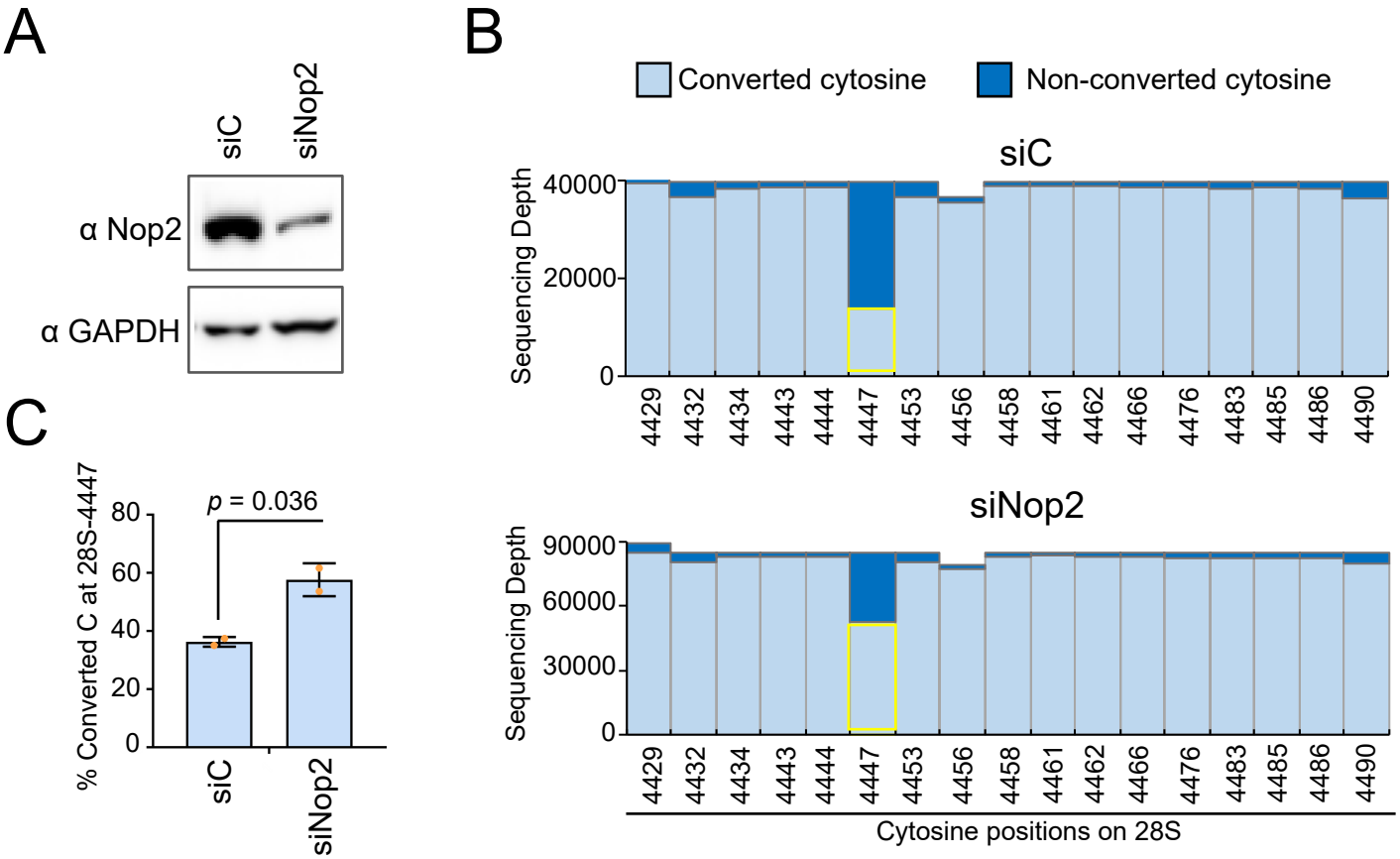

bioRxiv preprint doi: https://doi.org/10.1101/2021.11.12.468419; this version posted November 13, 2021. The copyright holder for this preprint (which was not certified by peer review) is the author/funder. All rights reserved. No reuse allowed without permission.

Liao et al., Fig.5

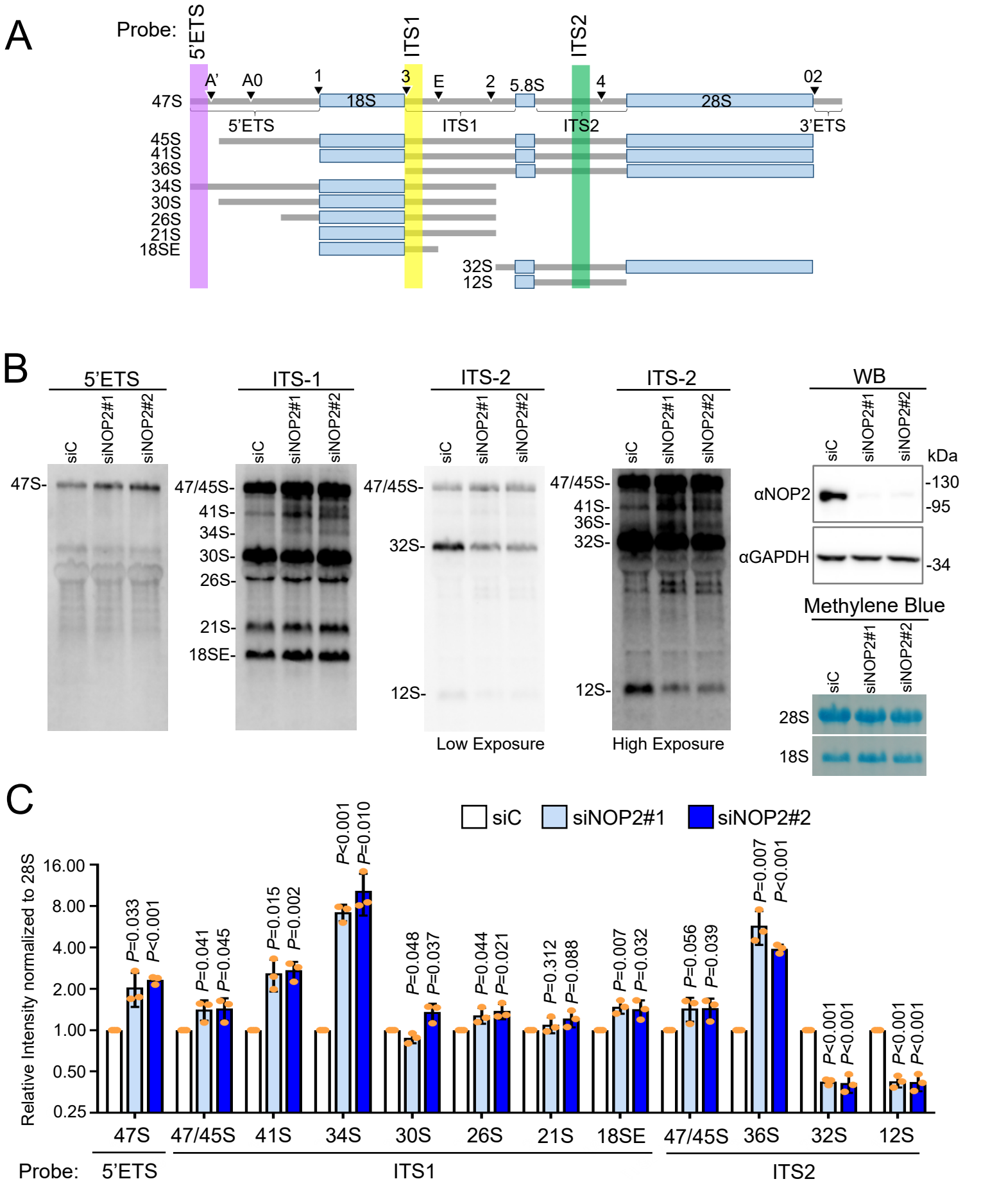

bioRxiv preprint doi: https://doi.org/10.1101/2021.11.12.468419; this version posted November 13, 2021. The copyright holder for this preprint (which was not certified by peer review) is the author/funder. All rights reserved. No reuse allowed without permission.

Liao et al. Fig. 6

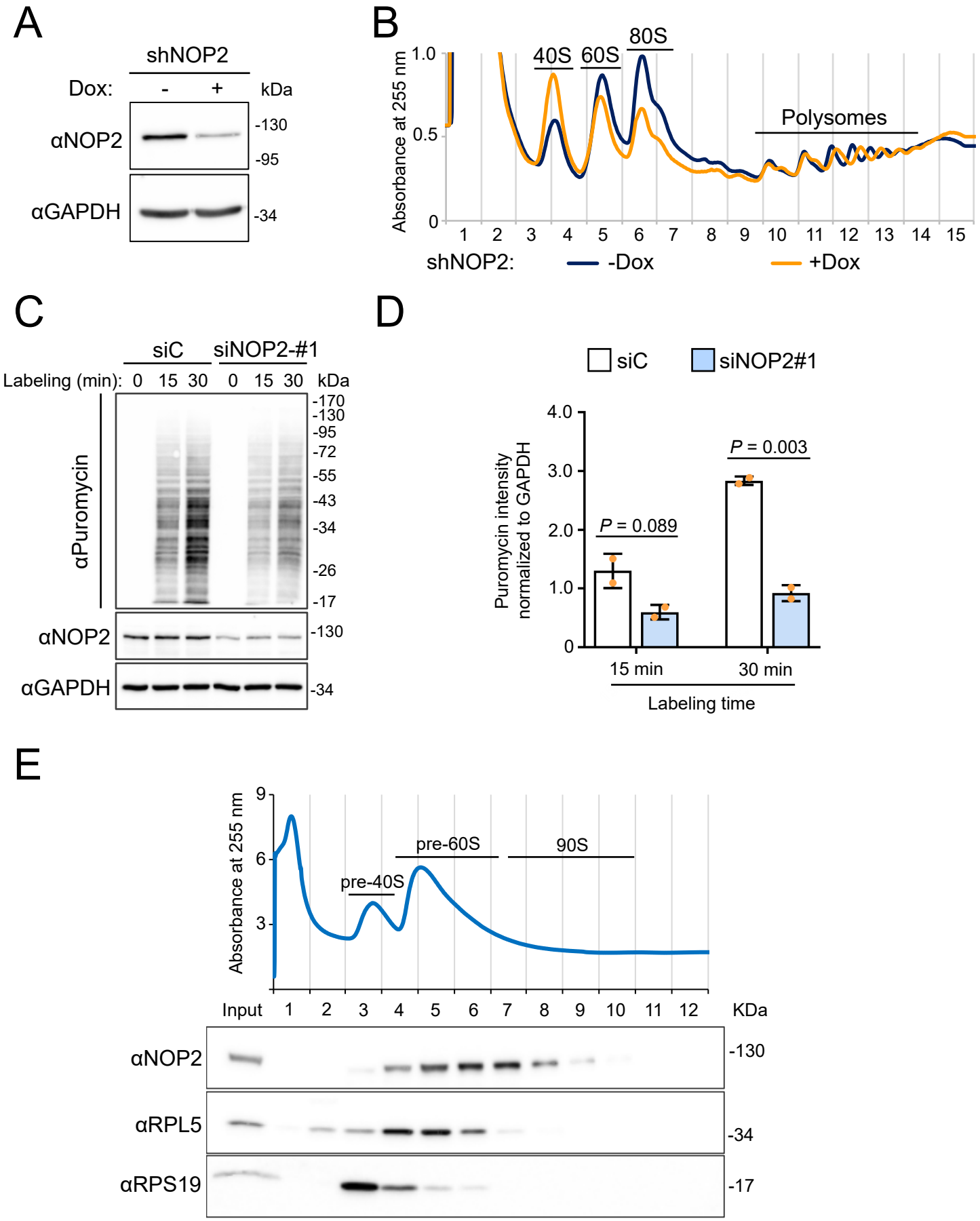

bioRxiv preprint doi: https://doi.org/10.1101/2021.11.12.468419; this version posted November 13, 2021. The copyright holder for this preprint (which was not certified by peer review) is the author/funder. All rights reserved. No reuse allowed without permission.

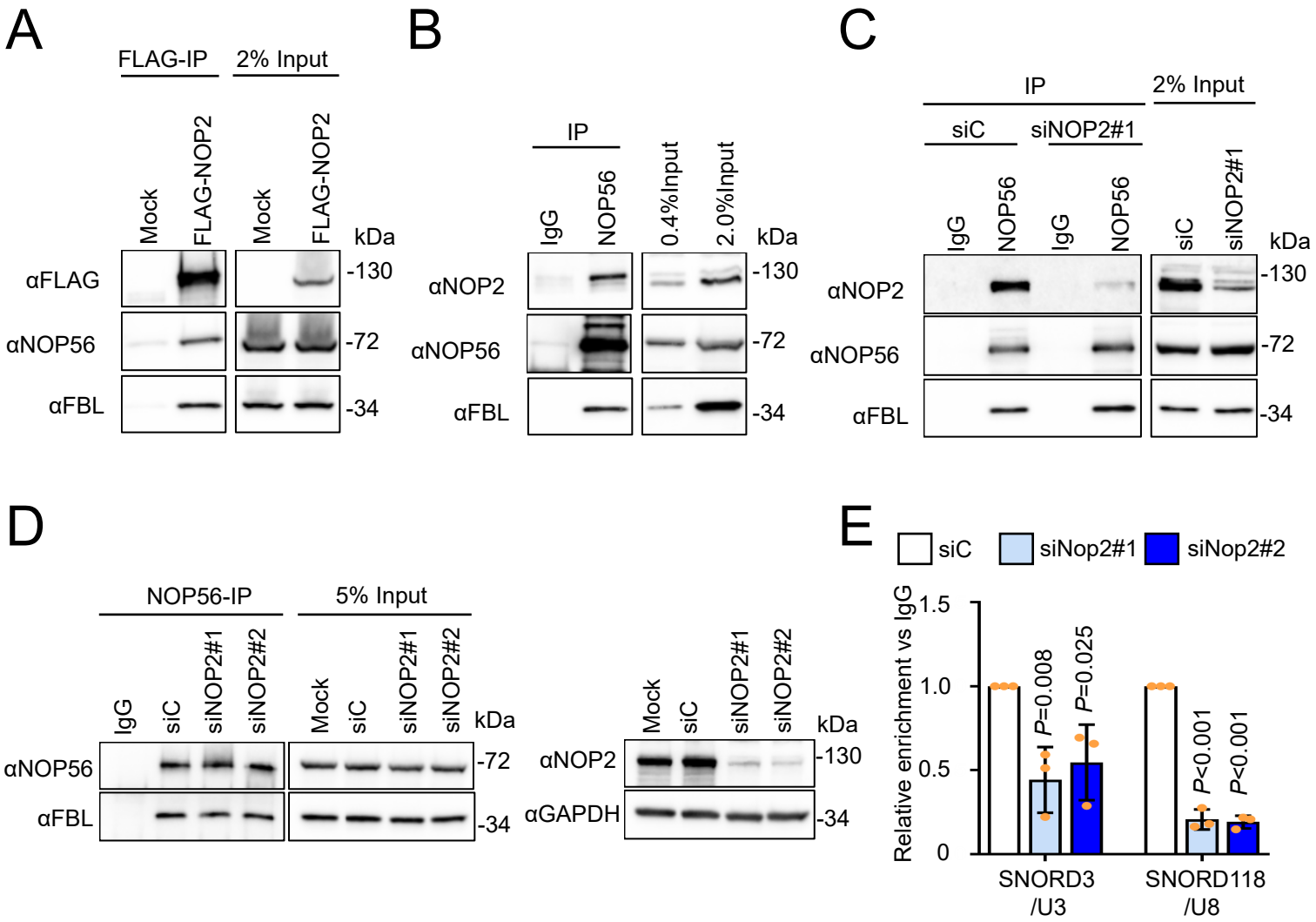

bioRxiv preprint doi: https://doi.org/10.1101/2021.11.12.468419; this version posted November 13, 2021. The copyright holder for this preprint (which was not certified by peer review) is the author/funder. All rights reserved. No reuse allowed without permission.

Liao et al., Fig.S1

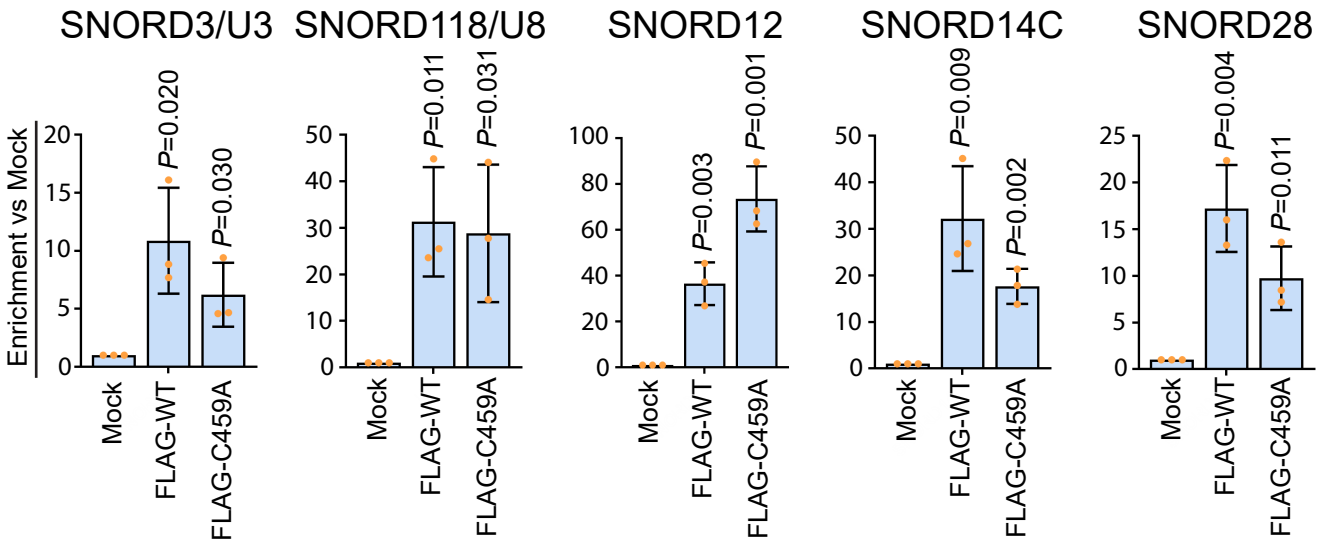

bioRxiv preprint doi: https://doi.org/10.1101/2021.11.12.468419; this version posted November 13, 2021. The copyright holder for this preprint (which was not certified by peer review) is the author/funder. All rights reserved. No reuse allowed without permission.

Liao et al., Fig.S2

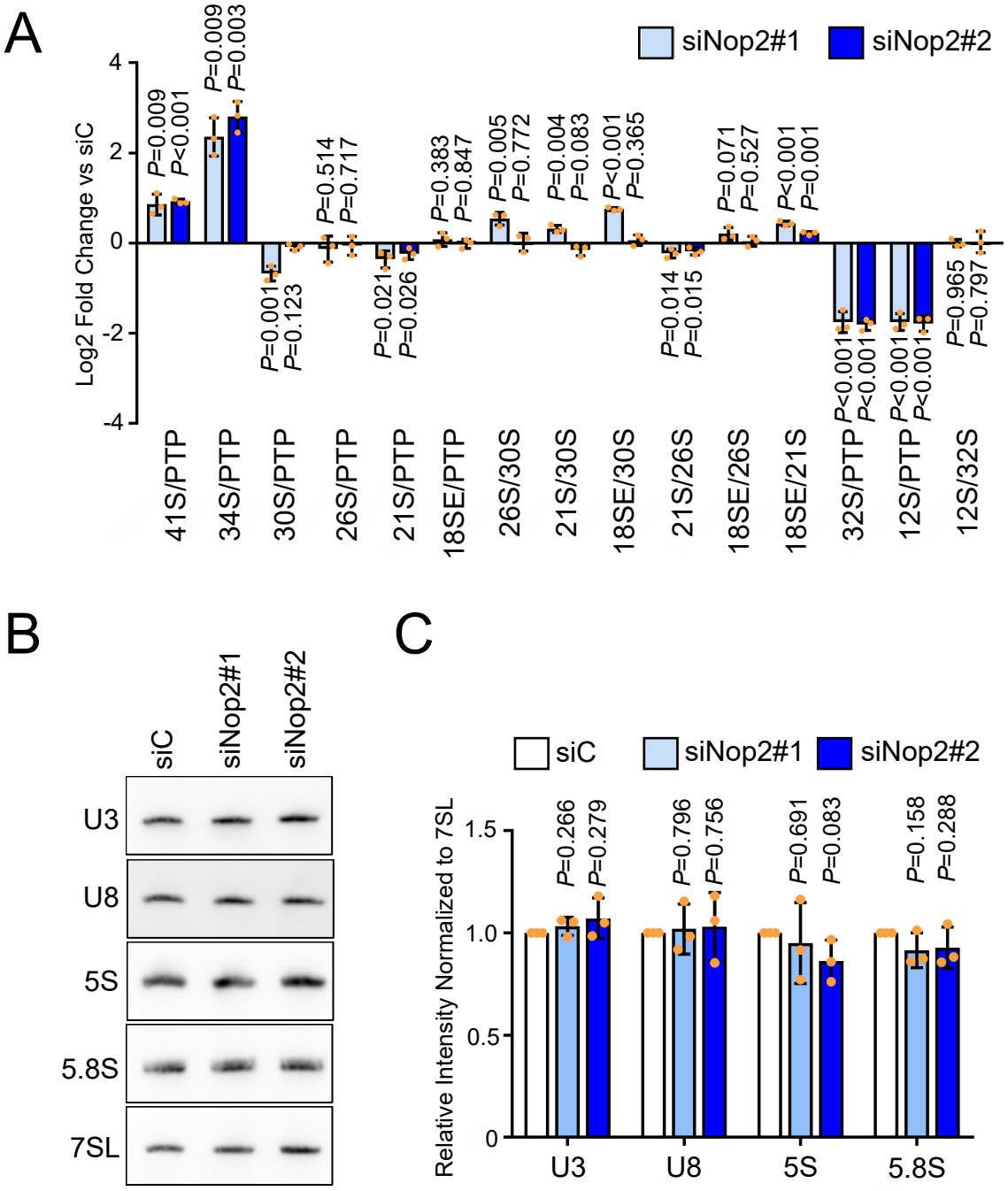

bioRxiv preprint doi: https://doi.org/10.1101/2021.11.12.468419; this version posted November 13, 2021. The copyright holder for this preprint (which was not certified by peer review) is the author/funder. All rights reserved. No reuse allowed without permission.
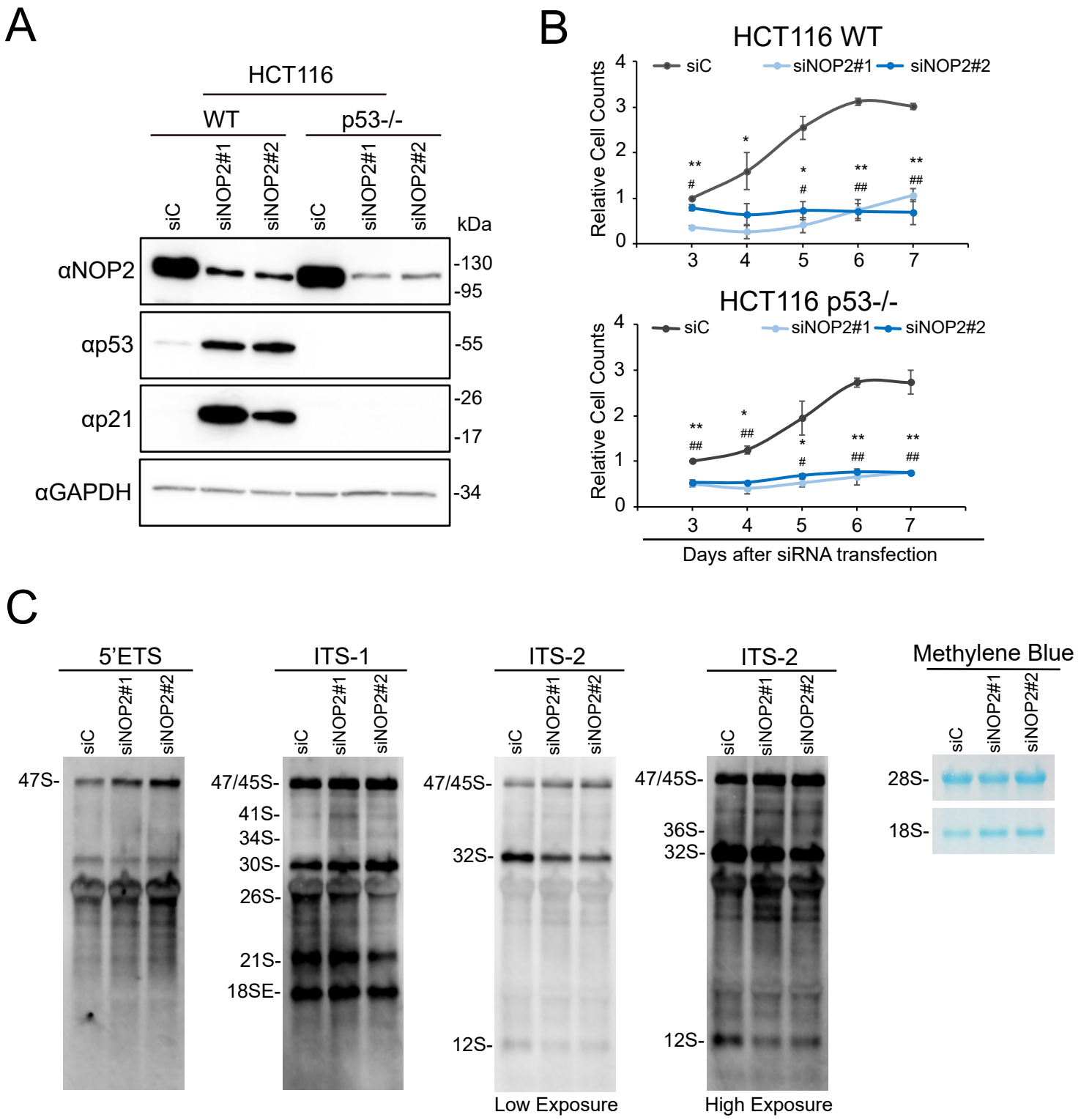
Liao et al., Fig S3